A New Population of Ultra-long Duration Gamma-ray Bursts

The Astrophysical Journal, 781:13 (22pp), 2014 January 20 doi:10.1088/0004-637X/781/1/13

A NEW POPULATION OF ULTRA-LONG DURATION GAMMA-RAY BURSTS

A. J. Levan[1], N. R. Tanvir[2], R. L. C. Starling[2], K. Wiersema[2], K. L. Page[2], D. A. Perley[3,26], S. Schulze[4,5], G. A. Wynn[2], R. Chornock[6], J. Hjorth[7], S. B. Cenko[8], A. S. Fruchter[9], P. T. O'Brien[2], G. C. Brown[1], R. L. Tunnicliffe[1], D. Malesani[6], P. Jakobsson[10], D. Watson[6], E. Berger[6], D. Bersier[11], B. E. Cobb[12], S. Covino[13], A. Cucchiara[14], A. de Ugarte Postigo[6,15], D. B. Fox[16], A. Gal-Yam[17], P. Goldoni[18], J. Gorosabel[15,19,20], L. Kaper[21], T. Krühler[6], R. Karjalainen[22], J. P. Osborne[2], E. Pian[23,24], R. Sánchez-Ramírez[15], B. Schmidt[25], I. Skillen[22], G. Tagliaferri[13], C. Thöne[15], O. Vaduvescu[22], R. A. M. J. Wijers[21], and B. A. Zauderer[6]

[1] Department of Physics, University of Warwick, Coventry CV4 7AL, UK; a.j.levan@warwick.ac.uk
[2] Department of Physics and Astronomy, University of Leicester, University Road, Leicester LE1 7RH, UK
[3] Department of Astronomy, California Institute of Technology, MC 249-17, 1200 East California Blvd., Pasadena, CA 91125, USA
[4] Pontificia Universidad Católica de Chile, Departamento de Astronomía y Astrofísica, Casilla 306, Santiago 22, Chile
[5] Millennium Center for Supernova Science
[6] Harvard-Smithsonian Center for Astrophysics, 60 Garden Street, Cambridge, MA 02138, USA
[7] Dark Cosmology Centre, Niels Bohr Institute, University of Copenhagen, Juliane Maries Vej 30, DK-2100 København Ø, Denmark
[8] Department of Astronomy, University of California, Berkeley, CA 94720-3411, USA
[9] Space Telescope Science Institute, 3700 San Martin Drive, Baltimore, MD21218, USA
[10] Centre for Astrophysics and Cosmology, Science Institute, University of Iceland, Dunhagi 5, IS-107 Reykjavk, Iceland
[11] Astrophysics Research Institute, Liverpool John Moores University, Egerton Wharf, Birkenhead CH41 1LD, UK
[12] Department of Physics, The George Washington University, Washington, DC 20052, USA
[13] INAF, Osservatorio Astronomico di Brera, Via E. Bianchi 46, I-23807 Merate, Italy
[14] Department of Astronomy and Astrophysics, UCO/Lick Observatory, University of California, 1156 High Street, Santa Cruz, CA 95064, USA
[15] Instituto de Astrofísica de Andalucía (IAA-CSIC), Glorieta de la Astronomía s/n, E-18008 Granada, Spain
[16] Department of Astronomy and Astrophysics, Pennsylvania State University, University Park, PA 16802, USA
[17] Department of Particle Physics and Astrophysics, Faculty of Physics, The Weizmann Institute of Science, Rehovot 76100, Israel
[18] APC, Astroparticule et Cosmologie, Universit Paris Diderot, CNRS/IN2P3, CEA/IRFU, Observatoire de Paris, Sorbonne Paris Cit, 10, rue Alice Domon et Leonie Duquet, F-75205 Paris Cedex 13, France
[19] Unidad Asociada Grupo Ciencia Planetarias UPV/EHU-IAA/CSIC, Departamento de Física Aplicada I, E.T.S. Ingeniería, Universidad del País Vasco UPV/EHU, Alameda de Urquijo s/n, E-48013 Bilbao, Spain
[20] Ikerbasque, Basque Foundation for Science, Alameda de Urquijo 36-5, E-48008 Bilbao, Spain
[21] Astronomical Institute Anton Pannekoek, University of Amsterdam, Science Park 904, NL-1098 XH Amsterdam, The Netherlands
[22] Isaac Newton Group of Telescopes, Apartado de Correos 321, E-38700 Santa Cruz de Palma, Spain
[23] Scuola Normale Superiore, Piazza dei Cavalieri 7, I-56126, Pisa, Italy
[24] INAF—Trieste Astronomical Observatory, via G. B. Tiepolo 11, I-34143 Trieste, Italy
[25] Research School of Astronomy and Astrophysics, The Australian National University, Weston Creek, ACT 2611, Australia
Received 2013 February 8; accepted 2013 October 28; published 2013 December 30

ABSTRACT

We present comprehensive multiwavelength observations of three gamma-ray bursts (GRBs) with durations of several thousand seconds. We demonstrate that these events are extragalactic transients; in particular, we resolve the long-standing conundrum of the distance of GRB 101225A (the "Christmas-day burst"), finding it to have a redshift $z = 0.847$ and showing that two apparently similar events (GRB 111209A and GRB 121027A) lie at $z = 0.677$ and $z = 1.773$, respectively. The systems show extremely unusual X-ray and optical light curves, very different from classical GRBs, with long-lasting, highly variable X-ray emission and optical light curves that exhibit little correlation with the behavior seen in the X-ray. Their host galaxies are faint, compact, and highly star-forming dwarf galaxies, typical of "blue compact galaxies." We propose that these bursts are the prototypes of a hitherto largely unrecognized population of ultra-long GRBs, which while observationally difficult to detect may be astrophysically relatively common. The long durations may naturally be explained by the engine-driven explosions of stars of much larger radii than normally considered for GRB progenitors, which are thought to have compact Wolf–Rayet progenitor stars. However, we cannot unambiguously identify supernova signatures within their light curves or spectra. We also consider the alternative possibility that they arise from the tidal disruption of stars by massive black holes and conclude that the associated timescales are only consistent with the disruption of compact stars (e.g., white dwarfs) by black holes of relatively low mass ($<10^5\ M_\odot$).

Key words: galaxies: distances and redshifts – gamma-ray burst: general – gamma-ray burst: individual (GRB 101225A, GRB 111209A, GRB 121027A)

Online-only material: color figures

1. INTRODUCTION

Classical long-duration gamma-ray bursts (GRBs) are active over timescales[27] ranging from ∼2 s up to several hundred seconds in the observer frame. In the context of the conventional collapsar model, this period is thought to reflect the initial lifetime of the ultra-relativistic jet, which, once it has drilled through to the surface of the stripped-envelope progenitor star, goes on to produce the "prompt" phase of high-energy emission (e.g., Bromberg et al. 2012).

[26] Hubble Fellow.
[27] Conventionally, GRB duration is most often quantified as the period, t_{90}, over which 90% of the γ-ray emission is observed (e.g., Kouveliotou et al. 1993). Strictly speaking, this is dependent on the sensitivity and bandpass of the detecting instrument (e.g., Qin et al. 2013).

Over the years, a small number of apparently even longer events have been observed; for example, GRB 970315 had $t_{90} \approx 1360$ s and was one of several bursts (out of ∼3000) with $t_{90} > 500$ s discovered by the *Compton Gamma-Ray Observatory* (*CGRO*)/Burst and Transient Source Experiment (BATSE; e.g., Tikhomirova & Stern 2005), although in most cases the very long duration was due to the tail of emission for extremely bright fast-rise-exponential-decay bursts, such as GRB 971208 (Giblin et al. 2002). Other instruments have also seen very long events, including the 1600 s GRB 020410 detected by BeppoSAX (Nicastro et al. 2004; Levan et al. 2005) and GRB 060814B detected by Konus-*WIND* (Pal'Shin et al. 2008). For all missions, such bursts appear to be extremely rare events, although the ability of a given instrument to find such bursts is a strong function of the detector characteristics and trigger algorithms as well as the observing scheme adopted. *Swift* has only seen a handful of GRBs with comparably long durations. In two cases, XRF 060218 (e.g., Pian et al. 2006; Campana et al. 2006; Soderberg et al. 2006) and XRF 100316D (e.g., Starling et al. 2011; Chornock et al. 2010a), these turned out to be low-redshift, low-luminosity explosions whose nature appears distinct from the bulk of cosmological GRBs (e.g., Soderberg et al. 2004, 2006; Liang et al. 2007; Chapman et al. 2007), although such events provide some of the best evidence for the association of GRBs with broad-lined type Ic supernovae (SNe; Pian et al. 2006; Bufano et al. 2012).

Interest in the nature of very long GRBs has been brought to the forefront by a series of recent discoveries by *Swift*. GRB 101225A (the so-called "Christmas-day burst") was active when *Swift* first slewed to the field (Palmer et al. 2010) and remained so for several thousand seconds longer (Thöne et al. 2011). Indeed, its properties were sufficiently unusual that two entirely different models for its origin have been proposed. In the first, the burst arises from the tidal shredding of an asteroid by a neutron star within our own Galaxy (Campana et al. 2011), while the second posits an extragalactic burst, associated with an SN inside a dense envelope at $z = 0.33$ (Thöne et al. 2011). The obstacle to further progress was the lack of a robust determination of its distance.

In another case, that of GRB 110328A/Swift J1644+57, the prompt phase spanned several days and has been argued to most likely be a tidal disruption event (TDE) produced when a star is consumed by a supermassive black hole (e.g., Levan et al. 2011; Bloom et al. 2011; Burrows et al. 2011; Zauderer et al. 2011b). An important piece of supporting evidence for this interpretation was the precise spatial coincidence of the outburst with the nucleus of its host galaxy (Levan et al. 2011; Zauderer et al. 2011b). However, it should be noted that this event has provoked lively debate and some collapsar-like models have been proposed as alternative explanations (Quataert & Kasen 2012; Woosley & Heger 2012); the total energetics are comparable in both scenarios (i.e., around the rest-mass energy of a star).

In this paper, we present evidence for another distinct class of ultra-long duration GRBs. We analyze new observations and spectroscopy of GRB 101225A, the prototype of this class and use extensive multiwavelength observations to show that GRB 111209A is similar (see also the recent paper by Gendre et al. 2013). Other members of the same class may also be present within the *Swift* sample and we discuss the recent GRB 121027A as a likely example of such an event. The paper is structured as follows: we investigate the high-energy properties and X-ray light curves and spectra of the bursts in Section 2 and then present spectroscopy and imaging to establish distances (Section 3), optical light curves (Section 4), and host galaxy properties (Section 5); from this, we consider constraints that can be placed on their progenitors. Throughout, we focus particularly on GRB 101225A and 111209A, since these are at a lower redshift and are better studied (Section 7). Finally, in Section 8, we consider whether other examples might exist within the archival *Swift* population, which have been unrecognized to date.

2. HIGH-ENERGY PROPERTIES

2.1. Prompt Emission

As discussed above, when initially discovered, both GRB 101225A and GRB 111209A stood out as being of remarkably long duration. In fact, in each case the detection by *Swift* was made as an "image trigger"; in other words, the flux detected by the Burst Alert Telescope (BAT) did not itself rise above the rate threshold,[28] but instead a statistically significant source was found in the reconstructed image plane.[29] It is worth noting that in the case of GRB 111209A this image trigger criterion was actually reached on two separate occasions, making it one of very few bursts that have triggered the instrument multiple times (Palmer et al. 2011).[30]

In the case of GRB 121027A, the prompt emission was sufficient to provide a standard "rate" trigger of the BAT (Barthelmy et al. 2012), but continued at a lower level for several thousand seconds beyond this point (R. L. C. Starling et al., in preparation).

One consequence of the differing modes of detection is that the trigger time becomes particularly poorly constrained for image triggers. The instrument only registers a detection at the end of the image trigger period, which can be significantly after the onset of bursting activity. Determination of the early power-law decay rate of the light curve, for example, depends on the assumed start time of the event and so will be less certain for these events than more typical GRBs. For all bursts considered in this paper, we utilize trigger times as reported by *Swift*, but note that these have significant uncertainties associated with them.

Estimating the duration of very long events is likewise not straightforward. First, they are active for much longer than the *Swift* orbit of ∼90 minutes (and at flux levels too faint for many other missions) and so there are periods of activity that are simply missed. Since GRBs are intrinsically highly variable, it is rarely possible to reconstruct the missing fluence over these gaps. This is important in these cases since the fluence is dominated not by the bright peaks at the beginning of the light curve (indeed, ultra-long bursts frequently do not have such peaks), but by the integration of the lower-luminosity, but much longer-lived, emission. In practice, this means that, especially in the absence of data from other observatories that do not suffer from Earth occultation, any attempt to determine a t_{90} will necessarily be crude. It should be noted that *Swift* has recently introduced a new trigger based on integrated fluence, which may increase the observed rates of these events.[31]

[28] Formally, there is not a single rate trigger, but several different rate-based triggering criteria.

[29] BAT is a very wide-field, coded-mask instrument. Most GRBs are initially identified by a rise in the overall count rate in the instrument (Gehrels et al. 2004).

[30] The very long event GRB 110328A/Swift J1644+57 also triggered the BAT on several occasions in this case over the space of ∼2 days.

[31] www.astro.ljmu.ac.uk/grb2012/presentations/presentations/gehrels_liverpool2012.pdf

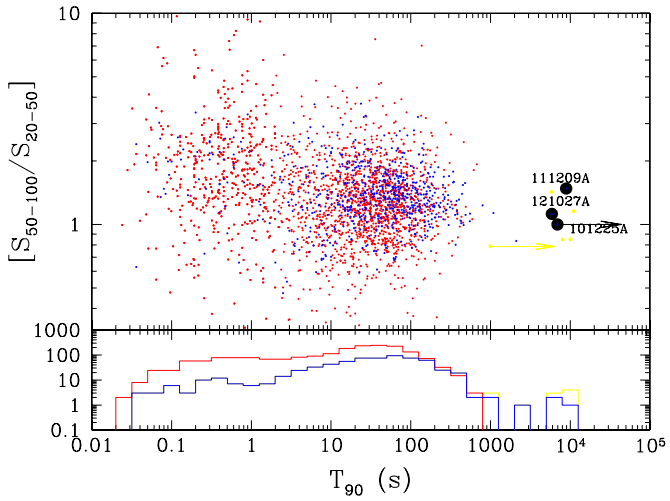

Figure 1. Spectral hardness (ratio of fluence in 50–100 keV over 20–50 keV) vs. duration diagram for *CGRO*/BATSE GRBs (red points) and *Swift* GRBs (blue points), with the locations of GRB 101225A, GRB 111209A, and GRB 121027A marked (note that these are approximate due to the lack of *Swift* orbit coverage). These three events have durations much longer than any seen by BATSE. In the case of GRB 101225A, the long-lived, low-level emission could easily have been missed, while GRB 111209A was seen as an extremely long burst by Konus-*WIND*. We also mark in yellow the location of other candidate ultra-long GRBs, in which the duration has been ascertained by the proxy of the time, or limits, on the rapid decay observed in the *Swift* XRT light curves. The lower panel shows a histogram of the observed durations, clearly identifying the location of the ultra-long bursts.

(A color version of this figure is available in the online journal.)

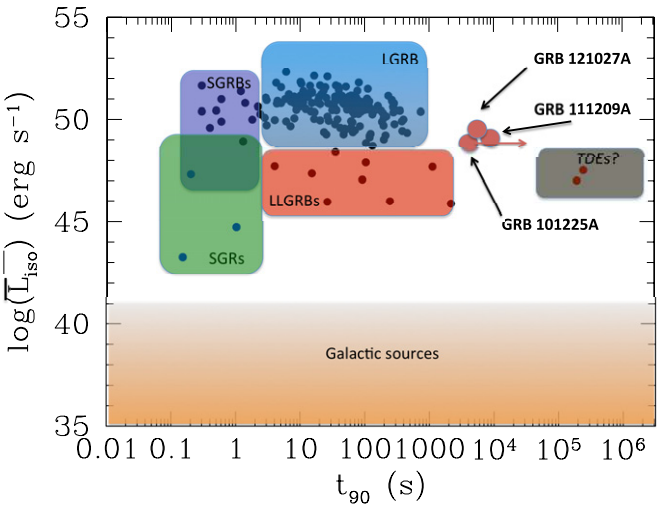

Figure 2. Parameter space for transients in the γ-ray sky, showing the duration of the burst and the approximate average luminosity over that duration. At low luminosity, there are numerous Galactic sources that we do not include in further detail; at higher luminosity, the outbursts for soft-gamma repeaters (SGRs) in our own Galaxy are shown, as well as extragalactic transients such as long- and short-duration GRBs (LGRBs and SGRBs) and the likely population of low-luminosity GRBs (LLGRBs). Two recently discovered very long transients, thought to be from TDEs, are also shown. The bursts considered in this paper (GRB 101225A, GRB 111209A, and GRB 121027A) are clearly outliers in any of these aforementioned classes.

(A color version of this figure is available in the online journal.)

In the case of GRB 101225A, we face the additional problem that the source was active when *Swift* first slewed to the location, so at best we have a lower limit on the duration. It was also clearly active in the subsequent *Swift* orbit (Thöne et al. 2011). This suggests a duration in excess of ∼7000 s. For GRB 111209A, there was fortunately also a detection from the Konus-*WIND* satellite in waiting mode (Golenetskii et al. 2011). This light curve clearly shows significant structure over a period of ∼10,000 s, including flaring activity while *Swift* was in Earth occultation. Finally, in the case of GRB 121027A, the burst is clearly detected in subsequent *Swift* orbits, at a rate a factor of ∼5 lower than the early peak (R. L. C. Starling et al., in preparation), again suggestive of a duration in excess of ∼6000 s, while observations with *MAXI* show ongoing activity during the *Swift* orbit gap (Serino et al. 2012). We adopt these durations as indicative of t_{90}, with the understanding that they are uncertain for the reasons outlined.

The approximate location of these events in the spectral hardness versus duration plane is shown in Figure 1 and in the average luminosity versus duration plane in Figure 2. Both views provide good illustrations of their extreme natures with respect to other GRBs and GRB-like populations.

2.2. X-Ray Light Curves

The X-ray (luminosity versus rest-frame time) light curves of all three GRBs are shown in Figure 3. All exhibit long-lived, high-luminosity activity, punctuated by large-scale dipping and flaring, followed by a rapid decline roughly $\sim 10^4$ s from the trigger. The bursts are detected in γ-rays during this plateau and appear to show a broad correlation between the γ-ray and X-ray emission (Thöne et al. 2011; Golenetskii et al. 2011; Gendre et al. 2013), albeit that the γ-ray detections are at a lower signal-to-noise ratio (S/N). In the cases of GRB 101225A and GRB 111209A, the light curves are strikingly similar, while GRB 121027A exhibits rather higher magnitude variability. The observed behavior is conspicuously unlike that seen in most GRBs (also shown), which typically fade rapidly on timescales of hundreds of seconds, followed by more slowly fading afterglow emission. While late-time activity is not especially unusual in GRB afterglows, manifesting as either flares (normally within the first thousand seconds) or long-lived plateaus (e.g., Zhang et al. 2006), the longevity of the emission at particularly high flux levels does make these bursts stand apart, as clearly seen in Figure 3. Below, we briefly discuss the quantitative properties of the ultra-long burst light curves.

For GRB 101225A, the light curve can be fit by a simple broken power law (of the form $F(t) \propto t^{-\alpha}$), with pre- and post-break indices of $\alpha_1 = 1.1^{+0.01}_{-0.01}$ and $\alpha_2 = 5.86^{+0.20}_{-0.19}$ and a break at $t_b = 22000 \pm 300$ s, although the pronounced dipping behavior means that the quality of the fit is relatively poor (χ^2/dof ∼ 3.6) and, given this, the error bars reported on the fit parameters should be treated with caution. We note that there is a hint of possible periodicity in the GRB 101225A light curve. Specifically, there is a sharp rise at the beginning of the second orbit of observation and a dip at the end of it. Similarly, there appear to be dips just at the end of the third and fourth orbits. This could be indicative repetitive behavior with a period around the *Swift* orbital period (or half of it). However, the small number of putative repeats within the observed data mean that no strong periodic signal can be recovered in the power spectrum of the X-Ray Telescope (XRT) light curve (Tanvir et al. 2011). Combined with the lack of any apparent periodicity in the light curves (γ-ray or X-ray) of the other two ultra-long bursts, we consider it most likely to be just coincidental in this case.

For GRB 111209A, the fits prefer a power law with three breaks, although again the fit statistics are significantly impacted by dipping and flaring behavior (with χ^2/dof = 7.5 in the final fit, where "dof" stands for degrees of freedom). In this case, we

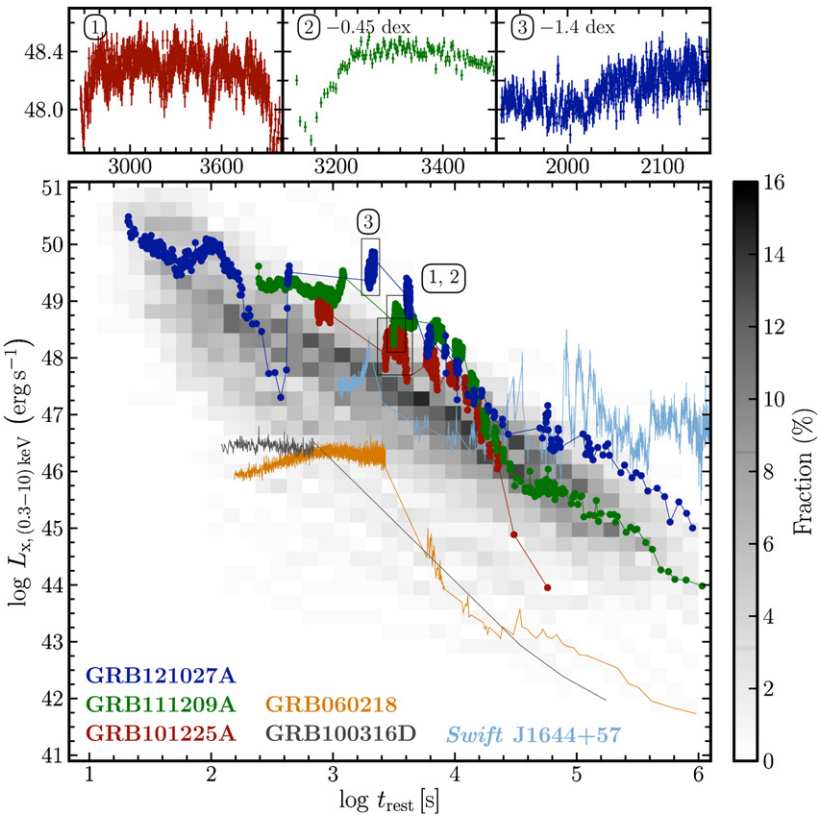

Figure 3. Rest-frame X-ray light curves of GRB 101225A (red), GRB 111209A (green), and GRB 121027A (blue), in luminosity space (rest frame 0.3–10 keV). There are compared with two well-known, very long GRBs (namely 060218 (orange) and 100316D (gray) and all *Swift* bursts with known redshifts (gray background shading). In light blue, we also show the light curve of Swift J1644+57 (Levan et al. 2011; Burrows et al. 2011), which persists for even longer, but is rather less luminous. The light curves of the ultra-long events are extremely similar, both in overall shape and the strong dipping behavior seen. The upper panels show the strong substructure present in the light curves of the ultra-long bursts, demonstrating rapid dipping with relatively narrow dips (in particular in the case of GRB 111209A). We also note that the luminosity of these events at late times ($\sim 10^4$ s) is substantially (a factor of $\sim$100) greater than that of typical GRBs. This is likely because the prompt emission in these cases persists for much longer, but clearly marks these events apart from other GRBs.

(A color version of this figure is available in the online journal.)

find the relevant slopes to be $\alpha_1 = 0.28^{+0.01}_{-0.01}$, $\alpha_2 = 0.77^{+0.01}_{-0.01}$, $\alpha_3 = 5.30^{+0.06}_{-0.06}$, and $\alpha_4 = 1.36^{+0.05}_{-0.05}$, with break times of $t_{b1} = 2050 \pm 20$ s, $t_{b2} = 16300 \pm 100$ s, and $t_{b3} = 46000 \pm 1000$ s. Although differing in details, the broad properties are very similar between the two bursts, in particular the timing, the presence of the steep decay index at times $>10^4$ s, and the slopes steeper than $\alpha \sim 5$. We note that in the case of GRB 111209A, the X-ray light curve returns to a typical afterglow decay value at the end of the steep slope. No such component is seen for GRB 101225A, although this may be due to the observations being of insufficient depth.

The light curve of GRB 121027A is somewhat different: it appears to show an early flare with a rapid decline, followed by a very rapid renewing of the activity around 1000 s after the initial trigger, persisting at a similar flux for the next 10^4 s before entering a rapid decay phase $\alpha = 4.60^{+0.18}_{-0.14}$, rather similar to GRB 101225A and 111209A. This is followed by a shallower decay, $\alpha = 0.47^{+0.11}_{-0.33}$, before entering a final decay ($\alpha = 1.44^{+0.08}_{-0.08}$) after 140 ks; this late-time decay is rather typical of GRB X-ray afterglows at these times post-burst (e.g., Evans et al. 2009).

In addition to the overall morphology of the X-ray emission, a striking feature of the bursts is the rapid apparent dipping and flaring behavior (some specific examples are shown in the inset panels in Figure 3). At these times, the emission fades or brightens by a factor >10–100 on timescales of $\sim$100 s. These temporal changes are unusual in GRB afterglows, but are rather typical in GRB prompt emission, which is seen to be highly variable. Indeed, the rapidity of the flux change, $\Delta t/t \sim 0.01$ in several cases, is typical of the expectations of ongoing prompt-like emission (e.g., Ioka et al. 2005). This change in flux is accompanied by a change in the X-ray spectral slope, with brighter periods corresponding to harder emission, the same general spectral evolution as seen in GRB prompt emission (e.g., Dezalay et al. 1997). Finally, if we interpret the early X-ray flux as long-lived, prompt GRB emission, then the rapid decay at the end of this activity could correspond to the observation of high-latitude emission, as is seen with similar decay slopes, but at much earlier times, in many "normal" GRBs (e.g., Kumar & Panaitescu 2000; Zhang et al. 2006, 2007, 2009).

2.3. X-Ray Spectroscopy

The bright and long-lived, high-energy emission provides high count rates for the *Swift* XRT, resulting in the possibility of detailed X-ray spectroscopy. However, this also represents a challenge in the sense that the early X-ray data ($<10^4$ s) exhibit substantial rapid variability and any changes in the X-ray spectra associated with this will complicate the fitting. We obtained time-sliced spectra from the UK Swift Science Data Centre GRB Repository[32] and grouped these such that a minimum of 20 counts populated each bin. The time slicing was made as fine as possible, following the variations in

[32] www.swift.ac.uk/xrt_spectra (Evans et al. 2007, 2009), processed using the *Swift* software released in HEASOFT 6.12.

Table 1
X-Ray Spectroscopic Fits of GRB 101225A

Time Slice	$N_{\rm H}$(int)	Photon Index	χ^2/dof
1390–1490	$0.38^{+0.11}_{-0.09}$	1.55 ± 0.06	193.96/159
1490–1590	0.32 ± 0.07	1.57 ± 0.06	164.60/169
1590–1690	$0.39^{+0.10}_{-0.09}$	$1.62^{+0.07}_{-0.06}$	159.76/150
1690–1755	0.4 ± 0.1	$1.72^{+0.09}_{-0.08}$	78.43/93
4950–5450	$0.58^{+0.10}_{-0.09}$	2.04 ± 0.06	200.08/204
5450–5950	0.37 ± 0.06	1.87 ± 0.05	234.04/230
5950–6450	0.32 ± 0.05	1.84 ± 0.05	221.75/228
6450–7269	$0.33^{+0.05}_{-0.04}$	1.90 ± 0.04	242.63/263
7272–7533	$0.20^{+0.19}_{-0.15}$	2.3 ± 0.3	11.97/11
10729–19093	0.15 ± 0.05	1.73 ± 0.06	132.35/159
22297–202625	$0.12^{+0.07}_{-0.06}$	$1.87^{+0.09}_{-0.08}$	87.03/92

Notes. The results of time-resolved X-ray spectroscopy of GRB 101225A. The time slices show the time since the BAT trigger, in seconds. We show the results for simple absorbed power-law fits to the data here, which provide an adequate quality of fit (χ^2/dof $\sim$ 1) for all but the earliest data. With the exception of this bin, there is no requirement for an additional component to be present in the data. Note the $N_{\rm H}$ is the intrinsic extinction, in addition to the Galactic component, and is given in units of 10^{22} cm^{-2}, at $z = 0.847$.

the decay rate, while obtaining a similar number of counts per spectrum. Spectra were fitted within Xspec 12.7.1, using chi-squared statistics. Galactic column densities were taken from the Leiden/Argentine/Bonn (LAB) H I Survey (Kalberla et al. 2005) and we adopted solar abundances from Anders & Grevesse (1989) and cross sections from Balucinska-Church & McCammon (1992). Intrinsic columns and blackbody parameters are measured in the source rest frame using the redshifts derived in Section 3. In photon counting mode, we fit all spectra over the energy range 0.3–10 keV. In window timing (WT) mode, we used the energy range 0.4–10 keV for GRB 101225A. In the XRT field of GRB 111209A, there are a number of X-ray sources. To minimize nearby source contributions to the WT mode spectra, we used the energy range 0.5–10 keV. Uncertainties are reported at the 90% confidence level.

In the case of GRB 101225A, the best-fitting spectral model for the early data was claimed to be a blackbody at a temperature of $\sim$1 keV, combined with a moderate intrinsic X-ray absorbing column (Thöne et al. 2011; Campana et al. 2011). However, this model works best predominantly at low redshift and is a somewhat worse fit at $z = 0.847$ (see below). Therefore, it is worthwhile to investigate the X-ray spectroscopy of both GRB 101225A and GRB 111209A in order to ascertain what spectral components may be at play and the consequences these may have for the nature of the bursts. Given the large-scale changes apparent in the spectra of both bursts, we chose to time slice the resulting data and fit the spectra separately within each time slice. For GRB 101225A, the time slices chosen are shown in Table 1. At all but the earliest times the spectra are adequately fit by a simple absorbed power law (albeit with a modest dispersion in the intrinsic absorption, $N_{\rm H}$, likely due to the degree of degeneracy between $N_{\rm H}$ and photon index), with the resulting fits also shown in Table 1. For the earliest data, which have a fit statistic of χ^2/dof = 193.96/159 for a power-law model, we investigate additional components. We find that several possible models introducing extra parameters can be used to improve the resulting fit, including the addition of a blackbody component, the use of a cutoff power law (as is often used in prompt GRB spectra), or the inclusion of a break in the power law, which might be appropriate to the early afterglow if a spectral break lies in the X-ray band. We discuss the implications of these models below.

For fits utilizing an additional blackbody, we find two broad minima in χ^2, with temperatures (in the rest frame) of $0.08^{+0.01}_{-0.02}$ and $1.40^{+0.3}_{-0.2}$ keV, respectively (both with good χ^2/dof of 152.25/157 and 152.16/157). This suggests a significant degree of degeneracy of the inferred temperature with other parameters, in particular the power-law slope and the intrinsic absorption. However, we also note that the higher temperature solution prefers a relatively low, but poorly constrained intrinsic absorption ($N_{\rm H} < 2 \times 10^{21}$ cm^{-2}) and hard underlying power law ($A(E) \propto E^{-\Gamma}$ with, $\Gamma \approx 1.4 \pm 0.2$) and would hence need significant evolution in both to be consistent with the later time spectrum.

A power law with an exponential high-energy cutoff also provides an adequate description of the data, which is of similar quality to either of the blackbody fits above with χ^2/dof of 151.92/158. However, this power law also requires a low $N_{\rm H}$, a very flat spectral slope with photon index $\Gamma = 0.5^{+0.2}_{-0.1}$, and a cutoff energy at $E_{\rm cut} = 3.1^{+1.0}_{-0.3}$ keV.

Similarly, a broken power law fits the break at around the same energy as the inferred cutoff above, $E_{\rm bk} = 3.1^{+0.7}_{-0.5}$ keV, with photon indices below and above the break of $\Gamma = 1.20^{+0.13}_{-0.16}$ and $\Gamma = 2.1^{+0.4}_{-0.3}$, respectively, again requiring a low $N_{\rm H}$. We note that the high-energy slope of $\sim$2.1 is consistent with the inferred slope of the early BAT observations $\Gamma = 1.82 \pm 0.32$, although with a large error. The inferred change of slope of $\Delta\Gamma = 0.9 \pm 0.4$ does not provide a strong discrimination of the possible nature of the break; a cooling break would imply $\Delta\Gamma = 0.5$, which is marginally consistent with the above break (although we note that the early-time optical spectral energy distributions (SEDs) of these events, in particular GRB 101225A (Thöne et al. 2011; Campana et al. 2011), show clear deviations from the expectations of a GRB fireball model.

Finally, we also attempt to fit a redshifted ionized absorbing model instead of the normal cold absorber. While not commonly used for GRBs, such models are frequently fit to active galactic nuclei (AGNs; e.g., George et al. 1998) and so may be appropriate if these events are some class of tidal disruption like flares. This also provides a good fit to the data, with the resulting fit having χ^2/dof = 146.46/157.

We adopt the same approach for our fitting of the GRB 111209A XRT spectra, slicing them broadly in time to sample both the long-lived plateau, the rapid decay, and late-time, afterglow-like emission. The choice of time slices and basic fit parameters are shown in Table 2. As with GRB 101225A, some time slices are inconsistent with a simple power law. Fitting these with an additional blackbody component provides an adequate fit at temperatures of either $kT = 0.13$ or 1.61 keV, with χ^2/dof = 728.75/712 and 703.25/712, respectively, for the time slice 800–1950 s after the burst. Broken and cutoff power-law models also provide an adequate fit to the data. In the case of a broken power law, the best-fit parameters (in the same time slice as above) are $\Gamma_1 = 1.18^{+0.02}_{-0.03}$, $\Gamma_2 = 1.59^{+0.04}_{-0.05}$, and $E_{\rm bk} = 3.51^{+0.20}_{-0.31}$ keV (χ^2/dof = 716.36/712), while for a cutoff power law, we find $\Gamma = 0.90^{+0.03}_{-0.03}$ and $E_{\rm cut} = 7.65^{+0.56}_{-0.49}$ keV, with χ^2/dof = 681.66/713.

In summary, for both GRB 101225A and GRB 111209A, we find that at early times there is significant deviation away from a simple power-law description of the data. This may imply an

Table 2
X-Ray Spectroscopic Fits of GRB 111209A

Time Slice	$N_{\rm H}$(int)	Photon Index	χ^2/dof
400–800	$0.39^{+0.02}_{-0.02}$	1.20 ± 0.01	700.83/613
800–1950	$0.37^{+0.01}_{-0.01}$	1.32 ± 0.01	908.56/714
1950–2060	$0.29^{+0.04}_{-0.03}$	1.02 ± 0.02	408.36/372
5000–6000	$0.32^{+0.02}_{-0.02}$	1.45 ± 0.02	385.44/420
6000–8000	$0.25^{+0.01}_{-0.01}$	1.58 ± 0.01	526.33/508
10000–20000	$0.29^{+0.01}_{-0.01}$	1.68 ± 0.01	604.92/563
10000–40000	$0.15^{+0.03}_{-0.02}$	1.74 ± 0.05	103.72/100
40000–2.16×10^6 s	$0.19^{+0.03}_{-0.03}$	2.39 ± 0.07	62.69/64

Notes. As for Table 1, but for GRB 111209A. The table shows the results of simple absorbed power-law fits. As can be seen, with the exception of the earliest data, these provide a generally adequate fit. Note the $N_{\rm H}$ is the intrinsic extinction, in addition to the Galactic component, given in units of 10^{22} cm^{-2} at $z = 0.677$.

unusually rapid variation in the underlying power-law spectrum that is not fully captured by our time-slicing approach, in the sense that the rapid flux variation might require the superposition of multiple power-law components, in which the impact of the absorption provides a turnover at low energies that can be fit as a blackbody peak or via other additional components. In this case, the better fits allowed by more complex models may simply be the consequence of adding additional parameters. However, we note that cutting down the spectra further in time results in fewer counts per spectrum and so also precludes the fitting of more complex models. We note that simply inferring the photon index from the hardness ratios (Evans et al. 2009) shows a high degree of rapid variability, often exhibiting $\Delta\Gamma \sim 0.5$ on timescales of only a few tens of seconds.[33]

Equally, we cannot rule out the possibility of an additional component in the X-ray spectra, but the data do not cleanly distinguish between blackbody, cutoff power laws, or broken power laws. We note that in most cases the fit statistic for these fits is χ^2/dof < 1, suggesting that, if anything, these models overfit the available data and hence we cannot strongly discriminate among different possible physical processes. Equally, since there are reasons that each may provide a reasonable physical explanation for the observed emission, we do not have a strong null hypothesis to prefer.

3. REDSHIFTS

Critical to any understanding of these events is, of course, their distance, something which was missing for all GRBs until the discovery of afterglows in the late 1990s. While a redshift determination was relatively straightforward for GRB 111209A, in the case of GRB 101225A it proved particularly problematic.

3.1. GRB 101225A

The distance of GRB 101225A has been a matter of significant debate since its initial discovery, with two mutually exclusive models being proposed to explain the event. In the first, the GRB is created by the tidal disruption and accretion of an asteroid mass of material onto a Galactic neutron star (Campana et al. 2011). In the second, the GRB is created by a massive star collapse inside a dense envelope (Thöne et al. 2011) at a redshift of $z \approx 0.33$, based on a photometric fit to the late-time light with a type Ic SN and the presence of significant X-ray absorption. The interpretation of the origin of this burst was complicated by its apparently featureless afterglow SED in the optical (Wiersema et al. 2010; Chornock et al. 2010b; Thöne et al. 2011), moderately low Galactic latitude ($b = -17^\circ$), and a position <100 kpc in projection from M31, if at the same distance as M31.

However, both pre-imaging and imaging obtained at late times after the burst show that there is a faint, coincident quiescent counterpart to GRB 101225A (Figure 4 and Thöne et al. 2011; McConnachie et al. 2009). We obtained Gemini GMOS spectroscopy of this source on 2012 July 19 and 20. In total, a 2.8 hr integration was obtained in nod and shuffle mode. These spectra were reduced through IRAF in the standard fashion and clearly show two emission lines at wavelengths of 6895 and 9263 Å, as well as further lower significance lines at 9000 and 9174 Å. These lines are naturally explained as being due to [O II], [O III], and Hβ at a common redshift of $z = 0.847$, thereby finally resolving the problem of the distance of GRB 101225A. This is a much larger luminosity distance than either of the previously proposed models, suggesting that neither fully captures the properties of the burst or progenitor. Cut-outs of the two-dimensional spectra around the lines are shown in Figure 4. In addition to these observations, the host of GRB 101225A has been observed by the Gran Telescopio Canarias (GTC) in 2012 July and August. These spectra confirm our redshift of $z = 0.847$ and will be presented in C. C. Thöne et al. (in preparation).

We also re-examined early spectra of the afterglow of GRB 101225A with this redshift in hand. These spectra were obtained from the William Herschel Telescope (WHT) with ACAM on 2010 December 26 and ISIS on 2010 December 27, with the MMT (Schmidt et al. 1989) on 2010 December 29, and from Gemini-N with GMOS on 2010 December 30. A complete log is shown in Table 3. We examined each of these spectra individually and compared them with a high S/N composite long-GRB afterglow spectra (Christensen et al. 2011), as shown in Figure 4. While some possible extremely weak features are visible (i.e., as troughs that overlap absorption features in the composite afterglow), this comparison suggests that the spectra were not of sufficient S/N for significant features to be seen, unless they were particularly strong, and so their non-detection is not indicative of a particularly unusual environment.

3.2. GRB 111209A

We obtained early spectroscopy of the transient optical light of GRB 111209A with both the Very Large Telescope (VLT)/X-shooter (2011 December 10 at 1:00 UT) and Gemini-N/GMOS-N. These spectra were processed through the standard pipelines for each instrument and show both absorption lines and emission lines from the host galaxy, providing a redshift of $z = 0.677$ (Vreeswijk et al. 2011). In addition, we obtained further spectroscopy from Gemini-S on the 2011 December 20 and X-shooter on 2011 December 27. A log of the ground-based spectroscopic observations of GRB 101225A and GRB 111209A is presented in Table 3 and images of the spectra can be seen in Figure 5.

These data are complemented by two *Hubble Space Telescope (HST)* grism spectra taken on 2011 December 20 and 2012 January 13, which are described in Section 4.2.

[33] See http://www.swift.ac.uk/burst_analyser/00509336/.

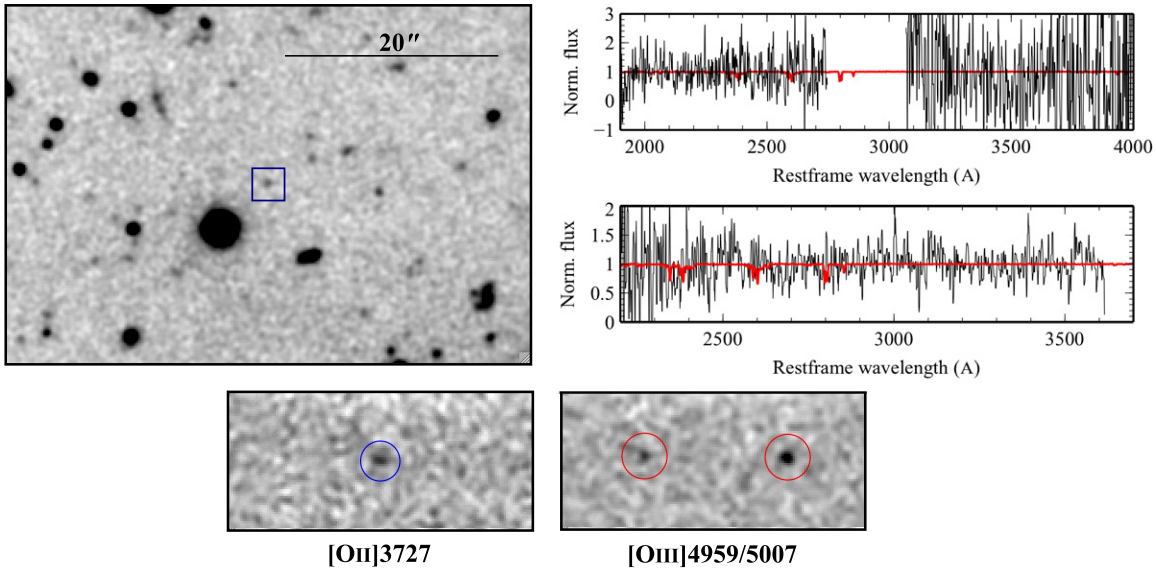

Figure 4. Observations of GRB 101225A. The upper left panel shows a finding chart of the region around the host galaxy (within the blue square). The image used is the late-time *g*-band observation made with Gemini-N/GMOS (north up and east to the left). The upper right panel shows our best afterglow spectroscopy, overlaid with a high S/N summed GRB afterglow template (red line from Christensen et al. 2011). The top sub-panel shows the WHT/ISIS data (the gap is between the blue and red arms) and the bottom one shows the Gemini/GMOS data. In neither case are absorption lines significantly detected, but this is not surprising given the S/N. The lower left and right panels show cut-outs of our late-time Gemini/GMOS two-dimensional spectroscopy of the host galaxy around the prominent oxygen emission lines (circled).

(A color version of this figure is available in the online journal.)

Table 3
Log of Ground-based Spectroscopic Observations of GRB 101225A, GRB 111209A, and GRB 121027A

Target	Date-obs	MJD-obs	ΔT (days)	Telescope	Exp. (s)	Spectral Range (Å)
101225A	2010 Dec 27	55557.005	1.23	WHT/ISIS	2400	5000–9000
101225A	2010 Dec 29	55559.175	3.40	MMT/Blue Channel	4800	3175–8385
101225A	2010 Dec 30	55560.205	4.43	Gemini-N/GMOS	3600	3868–6632
101225A	2012 Jul 19–20	56127.506	571.73	Gemini-N/GMOS	10240	5342–9458
111209A	2011 Dec 10	55905.036	0.74	VLT/X-shooter	4800	3000–25000
111209A	2011 Dec 10	55905.218	0.92	Gemini-N/GMOS	3600	3992–8108
111209A	2011 Dec 20	55915.153	10.85	Gemini-S/GMOS	1464	5992–10000
111209A	2011 Dec 29	55924.116	19.82	VLT/X-shooter	9600	3000–25000
121027A	2012 Oct 29	56229.253	1.94	Gemini-S/GMOS	2400	5200–7900
121027A	2012 Oct 30	56230.198	2.88	VLT/X-shooter	6000	3000–25000
121027A	2012 Oct 30	56230.199	2.89	Gemini-S/GMOS	2400	5200–7900

Notes. Ground-based spectroscopic observations of our sample of ultra-long GRBs, showing the telescopes and instrument setup used for each observation, along with its time since the initial *Swift* BAT trigger.

3.3. GRB 121027A

We obtained spectroscopy of GRB 121027A with Gemini-S/GMOS and with VLT/X-shooter on 2012 October 29 and 30. As above, full details are provided in Table 3. The GMOS observations were taken under poor conditions and have a limited wavelength range of ∼5200–7900 Å, but do show a strong absorption feature at 7770 Å, which was tentatively interpreted as the Mg II doublet at $z = 1.77$ (Tanvir et al. 2012). The X-shooter spectra span a much larger wavelength range and show multiple absorption lines from Mg, Fe, and Al species at a common redshift of $z = 1.773$, confirming our conclusion from the GMOS data (Kruehler et al. 2012). We note that the X-shooter observations also enable the detection of emission lines from the host galaxy in the infrared (IR) arm, specifically [O III] (4959, 5007), with other features lying in regions of high telluric absorption. A full description of these data will be presented in R. L. C. Starling et al. (in preparation).

4. ULTRAVIOLET, OPTICAL, AND INFRARED PROPERTIES

4.1. Swift UVOT Observations

In addition to our ground-based observations described below, the bright counterparts of both GRB 101225A and GRB 111209A were well detected in all of the bands of the *Swift* Ultraviolet and Optical Telescope (UVOT).

We use the UVOT data for GRB 101225A as given in Thöne et al. (2011). For GRB 111209A, we retrieved the data from the UK Science Data Centre. Image mode data were processed and analyzed using version 3.9 of the *Swift* software and the nominal 5″ aperture. The resulting photometry shows the source to be well detected in all bands at early times and visible in white light for ∼10 days after the initial outburst. The UVOT light curves are shown in Figure 6, while the derived photometry can be found in Table 4.

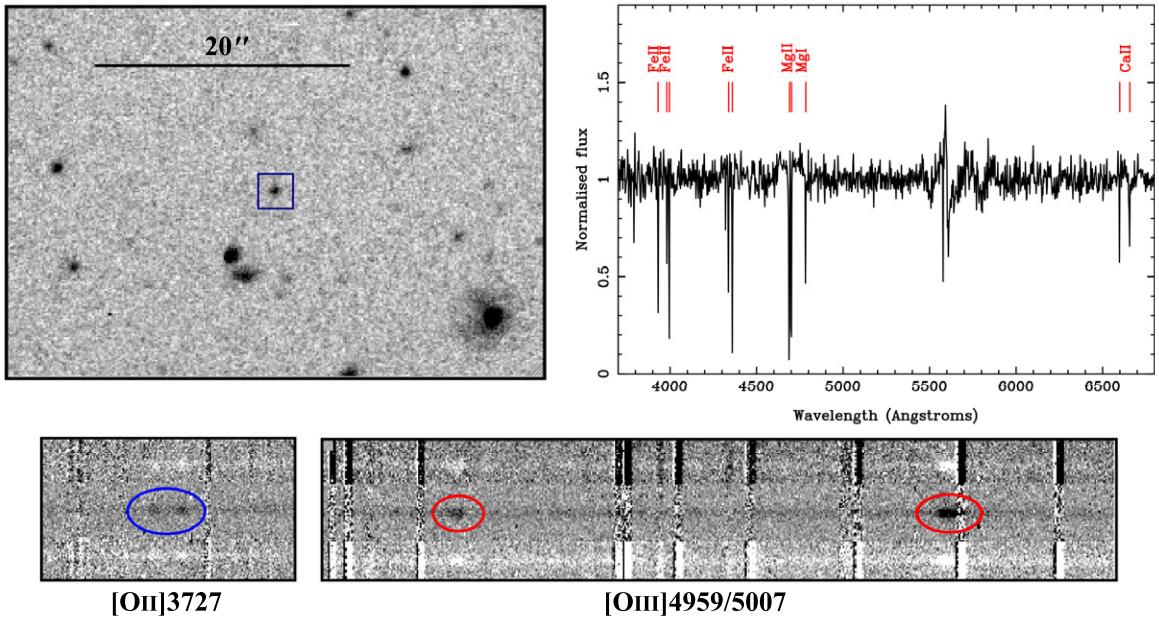

Figure 5. Finding chart and spectroscopy for GRB 111209A. The counterpart is shown in the blue box on an *HST* F125W image. The right spectrum shows a portion of the absorption spectrum obtained by X-shooter 0.74 days after the burst, demonstrating strong lines of Mg and Fe in the ISM of the host galaxy. The lower panels show the two-dimensional spectrum from X-shooter on 2011 December 29 and show strong emission lines from O II and O III (note that there is still a contribution from the afterglow, as seen in the continuum in these two-dimensional spectra).

(A color version of this figure is available in the online journal.)

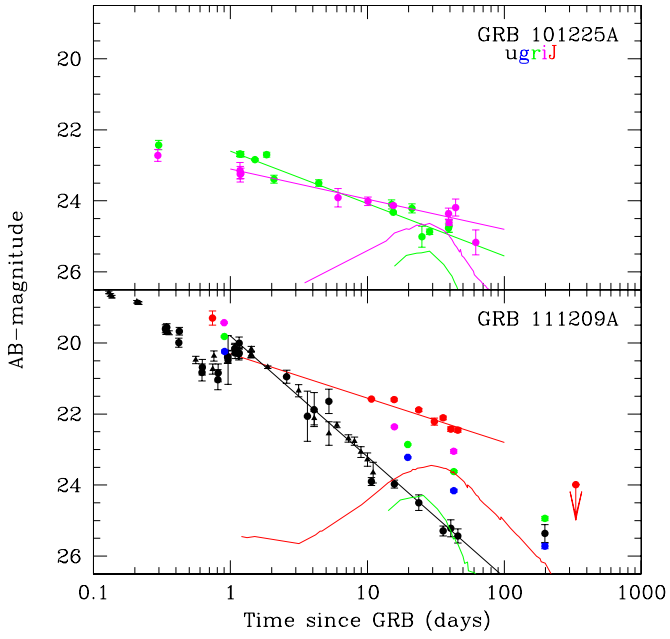

Figure 6. UV and optical light curve of GRB 101225A (top) and GRB 111209A (bottom). The colors represent the same filters in each panel, as shown by the inset key. We note that in the GRB 111209A panel we have represented the UVOT white light filter with the same color (black) as the *u* band given the similar central wavelength, but where the *u* band is indicated with circles, the white light points are marked as triangles. In addition, we show the inferred temporal slopes as solid lines for the *r* and *i* bands for GRB 101225A and for the *u* and *J* bands in GRB 111209A. The curves show the expectation for an SN 1998bw-like SN in the relevant band (colors coded as above) with no scaling or stretching. This is seen to be similar to the late-time magnitude of GRB 101225A, but well below the level seen in GRB 111209A.

(A color version of this figure is available in the online journal.)

GRB 121027A was only weakly detected by the UVOT with a white magnitude of 21.55 ± 0.25 in a 353 s exposure obtained between 77 s and 1192 s post-burst (Marshall & Evans 2012). In part, this lack of detection is likely due to the larger luminosity distance for GRB 121027A in comparison with GRB 101225A and GRB 111209A, while at $z = 1.773$ the bluest bands are also blueward of the Lyman limit.

4.2. HST Observations

4.2.1. GRB 101225A

GRB 101225A was observed with *HST* on 2011 January 13. At this epoch, we obtained a single orbit of observation, split between the F606W and F435W filters, using the Advanced Camera for Surveys (ACS). A full log of the data obtained is shown in Table 5. The data were processed through `multidrizzle`, after correction for the effect of pixel-dependent charge-transfer efficiency (CTE) and bias striping. In the resulting images, we clearly detect the counterpart of GRB 101225A with magnitudes of F606W $= 24.60 \pm 0.04$ and F435W $= 26.24 \pm 0.16$. These magnitudes are significantly above the host level (see below) in F606W and somewhat above the host in F435W. They imply that the observations contain a significant contribution from afterglow light.

In these data, the source is unresolved, being consistent with the *HST* point-spread function (PSF) at these wavelengths. A subtraction of a PSF reveals no significant residuals at the GRB location, suggesting the host is especially compact. We do note that there is a marginal elongation visible in the smoothed images (Figure 10), but that this is close to the limit of significance and is also along the direction of the read axis of the CCD (i.e., the direction in which any residual CTE is likely to act). At a redshift of $z = 0.847$, a size less than the *HST* PSF of 0.″08 implies a physical radius of less than 600 pc. This is a small galaxy, comparable to the most compact GRB hosts such GRB 060218 (e.g., Svensson et al. 2010).

4.2.2. GRB 111209A

We obtained two epochs of observations of GRB 111209A with *HST*/Wide Field Camera 3 (WFC3). The first was obtained

Table 4
Log of UVOT Observations of GRB 111209A

ΔT (s)	Exp. (s)	AB-mag	Error	Filter
742	19.5	19.03	0.26	UVW2
1021	19.5	19.87	0.39	UVW2
1369	19.5	19.84	0.38	UVW2
5344	197	19.66	0.12	UVW2
6780	197	19.67	0.11	UVW2
12398	886	19.64	0.06	UVW2
19034	694	19.93	0.07	UVW2
41800	886	20.92	0.11	UVW2
57659	660	21.30	0.17	UVW2
75113	886	21.75	0.20	UVW2
86682	886	21.33	0.14	UVW2
109615	886	21.31	0.15	UVW2
123155	366	21.56	0.23	UVW2
128450	886	21.09	0.12	UVW2
179202	315	22.34	0.48	UVW2
184866	315	22.66	0.63	UVW2
190594	315	22.05	0.40	UVW2
196414	315	22.13	0.42	UVW2
231066	315	22.58	0.60	UVW2
236842	315	22.34	0.49	UVW2
248391	315	22.68	0.62	UVW2
254167	315	22.52	0.60	UVW2
259893	315	21.66	0.31	UVW2
315812	1134	23.18	0.46	UVW2
347207	795	22.98	0.54	UVW2
453914	1820	22.92	0.30	UVW2
618	19.5	19.05	0.33	UVM2
791	19.5	19.28	0.38	UVM2
1593	19.4	19.66	0.45	UVM2
1768	19.5	19.03	0.33	UVM2
5754	197	19.91	0.17	UVM2
7190	197	19.06	0.11	UVM2
24053	886	19.75	0.07	UVM2
76528	91	21.06	0.55	UVM2
77083	110	20.69	0.34	UVM2
80922	886	20.89	0.14	UVM2
88370	629	20.96	0.16	UVM2
98094	886	20.94	0.15	UVM2
111387	793	20.99	0.14	UVM2
134472	823	21.65	0.21	UVM2
190934	180	21.93	0.64	UVM2
196724	120	21.52	0.56	UVM2
237248	310	21.46	0.33	UVM2
243230	816	21.96	0.29	UVM2
249516	1725	22.27	0.23	UVM2
255291	1725	22.43	0.26	UVM2
261042	1773	22.27	0.23	UVM2
347616	795	22.66	0.50	UVM2
454182	1820	22.76	0.33	UVM2
643	19.5	18.67	0.23	UVW1
816	19.5	18.58	0.23	UVW1
1095	19.5	18.90	0.26	UVW1
1269	19.5	19.12	0.29	UVW1
1444	19.5	18.74	0.24	UVW1
1618	19.5	19.47	0.36	UVW1
1793	19.5	18.78	0.25	UVW1
1966	19.5	19.38	0.34	UVW1
5959	197	19.64	0.13	UVW1
7396	197	18.87	0.08	UVW1
24836	642	19.74	0.07	UVW1
35663	886	20.36	0.09	UVW1
51634	374	21.12	0.30	UVW1
69284	886	21.15	0.17	UVW1
81829	886	20.84	0.12	UVW1
92290	886	20.76	0.14	UVW1

Table 4
(Continued)

ΔT (s)	Exp. (s)	AB-mag	Error	Filter
99001	886	20.60	0.10	UVW1
222045	2944	21.94	0.19	UVW1
315418	944	22.08	0.33	UVW1
348017	782	22.71	0.52	UVW1
454444	1680	22.99	0.42	UVW1
840	19.5	19.00	0.26	*U*
6164	197	19.12	0.09	*U*
7601	197	18.10	0.05	*U*
28976	295	19.60	0.11	*U*
29280	295	19.66	0.11	*U*
29583	295	19.56	0.10	*U*
36269	295	19.99	0.13	*U*
36568	285	19.67	0.11	*U*
53598	295	20.83	0.24	*U*
53895	282	20.69	0.22	*U*
69891	295	21.03	0.28	*U*
70186	279	20.84	0.25	*U*
82435	295	20.40	0.17	*U*
82738	295	20.38	0.17	*U*
92897	295	20.19	0.15	*U*
93200	295	20.15	0.14	*U*
93504	295	20.28	0.16	*U*
99607	295	20.31	0.16	*U*
99911	295	20.28	0.16	*U*
100152	172	20.01	0.17	*U*
222132	1341	20.95	0.18	*U*
352654	1148	21.88	0.48	*U*
451850	920	21.64	0.34	*U*
692	19.5	17.92	0.20	*B*
1144	19.5	18.12	0.23	*B*
1319	19.5	18.16	0.23	*B*
1494	19.5	18.32	0.26	*B*
1669	19.5	18.26	0.25	*B*
1842	19.5	18.79	0.37	*B*
2016	19.5	17.82	0.19	*B*
6369	197	18.88	0.12	*B*
7772	128	17.77	0.07	*B*
17006	295	18.43	0.11	*B*
17310	295	18.41	0.09	*B*
17613	295	18.44	0.08	*B*
29889	295	19.47	0.16	*B*
30194	295	19.32	0.14	*B*
30498	295	19.36	0.14	*B*
47562	295	19.86	0.21	*B*
47865	295	20.04	0.25	*B*
63209	295	20.20	0.47	*B*
63513	295	20.20	0.36	*B*
63816	295	20.32	0.32	*B*
93809	295	19.57	0.17	*B*
94113	295	20.12	0.26	*B*
94365	195	20.31	0.38	*B*
219341	1245	20.77	0.31	*B*
594	19.5	17.21	0.24	*V*
766	19.5	17.35	0.25	*V*
1046	19.5	17.76	0.33	*V*
1219	19.5	17.81	0.32	*V*
1394	19.5	17.29	0.24	*V*
1569	19.5	18.22	0.46	*V*
1743	19.5	17.88	0.35	*V*
1916	19.5	17.66	0.31	*V*
5549	197	18.04	0.16	*V*
6985	197	17.76	0.11	*V*
13005	295	18.12	0.11	*V*
13308	295	18.14	0.11	*V*
13538	148	18.46	0.20	*V*

Table 4
(Continued)

ΔT (s)	Exp. (s)	AB-mag	Error	Filter
22841	295	18.77	0.26	*V*
23144	295	18.75	0.20	*V*
23448	295	18.75	0.18	*V*
59628	295	19.68	0.37	*V*
75719	295	19.43	0.30	*V*
76023	295	19.66	0.37	*V*
87288	295	19.99	0.48	*V*
87591	295	19.13	0.23	*V*
87895	295	19.80	0.40	*V*
110221	295	19.52	0.33	*V*
110525	295	20.02	0.49	*V*
110828	295	19.70	0.38	*V*
129011	206	19.25	0.31	*V*
219752	760	20.65	0.57	*V*
502	147	18.74	0.04	White
717	19.5	18.12	0.08	White
931	147	18.53	0.04	White
1169	19.5	18.72	0.11	White
1343	19.5	18.68	0.11	White
1519	19.5	18.65	0.10	White
1693	19.5	18.80	0.11	White
1866	19.5	18.83	0.12	White
2040	19.5	18.22	0.08	White
657	197	18.97	0.04	White
11185	295	18.58	0.04	White
11489	295	18.65	0.04	White
11792	295	18.70	0.03	White
17918	295	18.83	0.04	White
18221.6	295	18.87	0.04	White
18525	295	18.881	0.04	White
30795	281	19.71	0.06	White
48143	237	20.48	0.10	White
64067	190	20.74	0.14	White
65539	98	20.37	0.14	White
122206	295	20.34	0.08	White
122509	295	20.32	0.08	White
122813	295	20.17	0.07	White
161758	4434	20.68	0.04	White
272116	511	21.34	0.17	White
353402	1148	22.12	0.19	White
452207	920	22.55	0.33	White
517782	10264	22.31	0.08	White
627714	10027	22.69	0.11	White
694819	9936	22.77	0.11	White
775015	9897	23.07	0.15	White
864545	9888	23.28	0.19	White
951132	7946	23.65	0.29	White

Notes. UVOT observations of GRB 111209A, taken in each of the UVOT filters. We have attempted to maintain separate magnitude measurements in each snapshot, where possible, in order to preserve the time series, but note that this occasionally leads to large (>0.3 mag) errors on the associated measurements.

on 2011 December 20 and the second on 2012 January 14. At each epoch, we obtained observations in two broadband filters, one ultraviolet (F336W) and one IR (F125W). In addition, we also obtained grism spectroscopy in G102 at each visit, covering the spectral range 0.8–1.15 μm.

The grism spectroscopy was processed through the `aXe` software that was used to background subtract, drizzle, and extract spectra of the afterglow at both epochs. The resulting grism spectra are shown in Figure 7 (note that in the second epoch, the central region has been removed and interpolated over due to contamination from the zeroth order of another star). The spectra show an apparent change in the spectral slope, from blue to red over the 20 day period between the two epochs of observation. This may be due to an underlying SN since the host galaxy light in the IR is apparently well below the measured magnitude at the time of our grism observations.

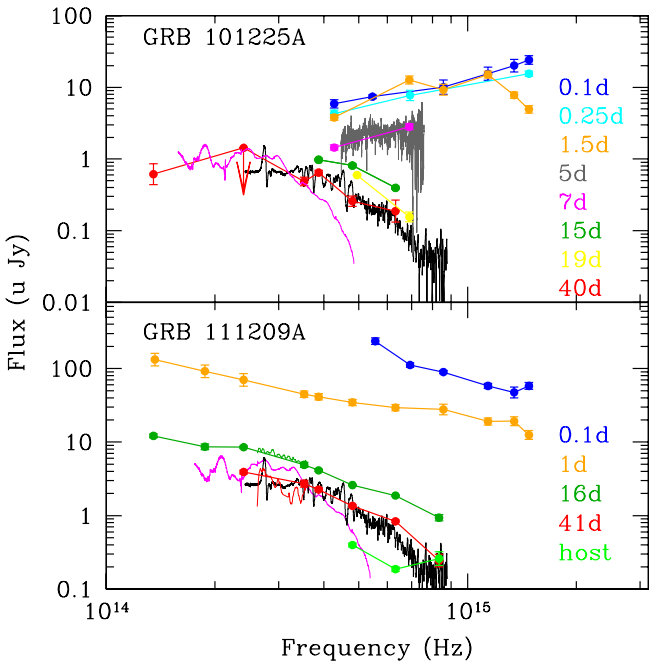

Figure 7. Evolution of the broadband SED of the afterglow of GRB 101225A (top) and GRB 111209A (bottom) over several epochs, as indicated. Spectroscopic observations of GRB 101225A with Gemini-N (gray) and GRB 111209A with the *HST* WFC3 grism are also plotted (at epochs 11 and 35 days after the bursts, color coded for the SED at that epoch). Both events show a blue-to-red evolution, although this is particularly strong in the case of GRB 101225A, which at early times shows a strongly rising SED toward the blue, possibly indicative of a thermal component peaking in the extreme-UV bands (Thöne et al. 2011). At late times, an SN 1998bw template (magenta, chosen to approximately match the same rest-frame epoch as the GRB data) does not provide a good fit to the global SED of either burst, suggesting that the SN underlying each could be rather different (SN 2005cs is shown in black as a template, which may represent the data). Alternatively, there could be an important contribution from any afterglow emission.

(A color version of this figure is available in the online journal.)

The optical and IR imaging was processed through multidrizzle in the standard fashion. At the two epochs, we measure magnitudes of F336W = 23.76 ± 0.04 and 25.58 ± 0.15 and F125W = 21.94 ± 0.02 and 22.18 ± 0.15 (all AB magnitudes). Our ground-based observations (see below) imply that at the time of our second *HST* epoch, the *u*-band light was dominated by the host galaxy and so we assume the host has F336W(AB) = 25.78 ± 0.15, whereas we assume the other magnitudes are dominated by transient light.

4.3. Ground-based Optical and Infrared Observations

4.3.1. GRB 101225A

We obtained several epochs of optical/near-IR imaging of GRB 101225A using Gemini-N/GMOS and NIRI[34] and WHT/ACAM. These observations were reduced via the standard pipelines. Photometric calibration in the *g* and *i* bands was performed relative to the PAndAS survey (McConnachie et al.

[34] Some of these data have been independently reported by Thöne et al. (2011).

Table 5
Log of *HST* Observations of GRB 101225A and GRB 111209A

Target	Date-obs	MJD-obs	ΔT	Filter	Exp. (s)	AB-magnitude
101225A	2011 Jan 13	55574.017	18.241	ACS/F606W	880	24.60 ± 0.04
101225A	2011 Jan 13	55574.034	18.258	ACS/F435W	1020	26.24 ± 0.16
111209A	2011 Dec 20	55915.435	11.135	WFC3/UVIS/F336W	1050	23.76 ± 0.04
111209A	2011 Dec 20	55915.452	11.152	WFC3/IR/F125W	1059	21.70 ± 0.02
111209A	2011 Dec 20	55915.504	11.204	WFC3/IR/G102	2212	...
111209A	2012 Jan 13	55939.458	35.157	WFC3/UVIS/F336W	1400	25.58 ± 0.15
111209A	2012 Jan 13	55939.455	35.154	WFC3/IR/F125W	153	22.18 ± 0.15
111209A	2012 Jan 13	55939.379	35.079	WFC3/IR/G102	3612	...

Notes. A log of the *HST* observations of each of GRB 101225A and GRB 111209A, showing instrument and filters used for each observation, along with the time since burst trigger and, where appropriate, the measured magnitude of the optical/IR counterpart.

Table 6
B- and *g*-band Magnitudes of Secondary Standard Stars in the GRB 101225A Field

REF	R.A.	Decl.	*g*	Err	*B* (AB)	Err
9	00:00:48.48	+44 36:19.3	19.88	0.02	20.89	0.1
10	00:00:47.98	+44:35:57.8	19.28	0.02	20.12	0.1
11	00:00:50.58	+44:35:43.5	19.10	0.02	19.88	0.1
12	00:00:51.59	+44:35:19.1	19.46	0.02	20.02	0.1
13	00:00:43.29	+44 35:13.1	18.32	0.02	18.89	0.1

Notes. Updated magnitudes for *g*-band secondary standard stars used in Thöne et al. (2011) and based on the native *g*-band calibration from the PAndAS survey. The reference number is the ID given in Thöne et al. (2011). The *i*-band calibration is broadly in keeping with that in Thöne et al. (2011) and so we adopt it here. Our *g*-band calibration has significantly smaller errors than that reported in Thöne et al. (2011), where the calibration was extrapolated from the Sloan Digital Sky Survey.

2009), which covered the same field. This has the advantage of being taken as a native calibration and has significantly smaller errors for the comparison stars than reported in Thöne et al. (2011), especially in the *g* band. For other optical bands, we adopt the calibration of Thöne et al. (2011) for consistency and in the IR we calibrate our observations relative to Two Micron All Sky Survey (2MASS). An updated photometric calibration for the *g* band is shown in Table 6. The resulting photometry in all bands is shown in Table 7.

The optical (*r* and *i* band) light curve of GRB 101225A is shown in Figure 6. Beyond one day, the *i* band can be adequately fit with a single power law with a slope of index $\alpha_i = 0.34^{+0.04}_{-0.05}$ (χ^2/dof = 2.696/6). Fitting a similar model to the better sampled *r*-band light curve provides a slope of $\alpha_r = 0.59^{+0.02}_{-0.02}$, but the resulting fit is poor (χ^2/dof = 36.92/11), indicative of a degree of additional variability. There is a notable plateau in the *r* band between ~15–40 days where the magnitude changed by $\Delta r = -0.39 \pm 0.19$. In the *i* band over the same frame, we see $\Delta i = -0.49 \pm 0.09$, slightly slower than the decay above. Both of these decay rates are very slow for GRB afterglows at these late times. A plausible explanation of the plateau and apparent reddening is the emergence of an SN, although the data are not strongly diagnostic of this (see the discussion). We note that the optical afterglow appears largely disconnected from the X-ray. There is no rapid decay coincident with the decay observed in the X-ray and the optical continues with a moderately shallow slope for many days, long after the source has become invisible to the XRT.

We also obtained a final late epoch of *g*-band observations with Gemini-N on 2011 July 1. At this time, we clearly detect a source with $g = 26.79 \pm 0.14$, similar to the magnitude inferred from pre-imaging of the field in PAndAS (Thöne et al. 2011); this is likely the host galaxy of GRB 101225A.

Table 7
Ground-based Photometric Observations of the GRB 101225A Afterglow

Date-obs	MJD-obs	ΔT (days)	Telescope	Band	Exp. (s)	AB-mag
2010 Dec 26	55556.9472	1.1710	WHT	*r*	300	22.68 ± 0.08
2010 Dec 26	55556.9517	1.1755	WHT	*i*	300	23.15 ± 0.25
2010 Dec 26	55556.9561	1.1799	WHT	*i*	300	23.25 ± 0.24
2010 Dec 26	55556.9600	1.8380	WHT	*r*	300	22.70 ± 0.07
2010 Dec 26	55556.9643	1.1880	WHT	*r*	300	22.69 ± 0.08
2010 Dec 26	55556.9683	1.1921	WHT	*i*	300	23.23 ± 0.16
2010 Dec 27	55557.2861	1.5100	Gemini	*r*	120	22.84 ± 0.03
2010 Dec 30	55560.1863	4.4101	Gemini	*r*	720	23.50 ± 0.10
2011 Jan 9	55570.8289	15.0527	WHT	*r*	1500	24.10 ± 0.14
2011 Jan 9	55570.8500	15.0732	WHT	*B*	3600	25.88 ± 0.40
2011 Jan 10	55571.2056	15.4293	Gemini	*g*	1200	25.22 ± 0.10
2011 Jan 10	55571.2229	15.4467	Gemini	*r*	1440	24.32 ± 0.03
2011 Jan 10	55571.2444	15.4682	Gemini	*i*	1890	24.13 ± 0.04
2011 Jan 19	55580.8419	25.0657	WHT	*r*	3600	25.01 ± 0.32
2011 Jan 23	55584.2674	28.4911	Gemini	*r*	900	24.87 ± 0.08
2011 Feb 3	55595.2632	39.4870	Gemini	*g*	900	26.25 ± 0.32
2011 Feb 3	55595.2486	39.4724	Gemini	*r*	900	24.71 ± 0.19
2011 Feb 3	55595.2347	39.4585	Gemini	*i*	900	24.62 ± 0.08
2011 Feb 3	55595.2181	39.4418	Gemini	*z*	1260	24.90 ± 0.25
2011 Jul 1	55743.5576	187.7810	Gemini	*g*	3000	26.79 ± 0.14

Notes. Photometric observations of GRB 101225A obtained at the WHT and Gemini-N. The magnitudes have not been corrected for Galactic extinction; to do so would require corrections based on Schlafly & Finkbeiner (2011) of $A_B = 0.37$, $A_g = 0.33$, $A_r = 0.23$, $A_i = 0.17$, and $A_z = 0.13$.

4.3.2. GRB 111209A

We obtained multiple epochs of imaging in the *ugrizJHK* bands from Gemini North, Gemini South, and the VLT. The Gemini images were processed as above, while the VLT observations were processed through the relevant European Southern Observatory imaging pipeline. The IR observations were calibrated against 2MASS stars lying within the field of view, while the optical images were calibrated against the photometric calibration used by GROND (D. A. Kann 2012, private communication). For the *u* band, we calibrate against the F336W *HST* images and confirm this calibration for brighter stars using the UVOT *u* band. The resulting photometry is shown in Table 8 and Figure 6.

The bluest bands (namely, the UVOT *u* band and white light and ground-based *u* band, which have similar central

Table 8
Ground-based Photometric Observations of the GRB 111209A Afterglow

Date-obs	MJD-obs	ΔT	Telescope	Band	Exp. (s)	Mag (AB)
2011 Dec 9	55905.2060	0.9059	Gemini-N	g	3×60	20.24 ± 0.04
2011 Dec 9	55905.2025	0.9024	Gemini-N	r	3×60	19.82 ± 0.02
2011 Dec 9	55905.1991	0.8990	Gemini-N	i	3×60	19.52 ± 0.02
2011 Dec 9	55905.1956	0.8955	Gemini-N	z	3×60	19.43 ± 0.02
2011 Dec 19	55915.0757	10.7756	Gemini-S	u	8×180	23.41 ± 0.08
2011 Dec 25	55920.0293	15.7292	VLT/FORS2	u	4×300	23.97 ± 0.10
2011 Dec 25	55920.0462	15.7461	VLT/FORS2	i	8×120	22.36 ± 0.03
2011 Dec 25	55920.0610	15.7609	VLT/FORS2	z	8×120	22.18 ± 0.08
2011 Dec 25	55920.0252	15.7251	VLT/HAWKI	J	35×60	21.59 ± 0.04
2011 Dec 25	55920.0611	15.7783	VLT/HAWKI	H	35×60	21.56 ± 0.09
2011 Dec 25	55920.0974	15.8164	VLT/HAWKI	K	38×60	21.19 ± 0.06
2011 Dec 29	55924.0348	19.7347	VLT/FORS2	g	4×250	23.22 ± 0.02
2011 Dec 29	55924.0484	19.7483	VLT/FORS2	R	4×250	22.86 ± 0.02
2012 Jan 2	55928.0362	23.7361	VLT/FORS2	u	6×300	24.50 ± 0.23
2012 Jan 2	55928.0264	23.7263	VLT/HAWKI	J	35×60	21.77 ± 0.04
2012 Jan 9	55935.1356	30.8355	VLT/HAWKI	J	35×60	22.21 ± 0.10
2012 Jan 14	55940.0406	35.7405	VLT/FORS2	u	4×300	25.29 ± 0.24
2012 Jan 14	55940.0173	35.7172	VLT/HAWKI	J	35×60	22.10 ± 0.05
2012 Jan 19	55945.0319	40.7318	VLT/FORS2	u	9×300	25.22 ± 0.24
2012 Jan 19	55945.0241	40.7240	VLT/HAWKI	J	35×60	22.43 ± 0.06
2012 Jan 21	55947.0652	42.7651	VLT/FORS2	g	4×250	24.16 ± 0.04
2012 Jan 21	55947.0787	42.7786	VLT/FORS2	R	4×250	23.62 ± 0.03
2012 Jan 21	55947.0351	42.7350	VLT/FORS2	i	8×120	23.05 ± 0.05
2012 Jan 21	55947.0499	42.7497	VLT/FORS2	z	8×120	22.84 ± 0.11
2012 Jan 24	55950.0425	45.7424	VLT/FORS2	u	9×300	25.44 ± 0.20
2012 Jan 24	55950.0275	45.7274	VLT/HAWKI	J	35×60	22.45 ± 0.06
2012 Jun 24	56102.4181	198.118	Gemini-S	u	5×300	25.36 ± 0.25
2012 Jun 24	56102.3876	198.088	Gemini-S	g	5×180	25.72 ± 0.07
2012 Jun 24	56102.4012	198.101	Gemini-S	r	5×180	24.94 ± 0.06
2012 November 6	56237.2979	332.998	Gemini-N	J	45×60	>24.0

Notes. Photometric observations of GRB 111209A obtained at Gemini-N, Gemini-S, and the Very Large Telescope. The magnitudes have not been corrected for Galactic extinction; to do so would require corrections based on Schlafly & Finkbeiner (2011) of $A_u = 0.08$, $A_g = 0.06$, $A_r = 0.04$, $A_i = 0.03$, $A_z = 0.02$, $A_J = 0.0013$, $A_H = 0.008$, and $A_K = 0.005$.

wavelengths) show a moderately steep decay. After the first day, we find that these bands exhibit a slope of $\alpha_{\rm white} = 1.38^{+0.06}_{-0.06}$ (χ^2/dof = 9.92/11), rather similar to the slope inferred from the X-rays at the same time ($\alpha_X = 1.36^{+0.05}_{-0.05}$), although we note that at early times, as with GRB 101225A, there is no strong correlation between the X-ray and optical light. The similarity of the late-time slopes suggests that these bands may well be exhibiting standard afterglow behavior. The spectral slope from X-rays to the u band at $\sim$1 day is $\beta_{\rm OX} \approx 1$, while the slope inferred from the X-ray alone is $\beta_X = 1.39 \pm 0.07$ (Table 2); these slightly different slopes do allow for a cooling break lying between the optical and X-ray, although this would be disfavored by the near-identical decay rates.

In contrast to the bluer bands, the redder optical and near-IR bands show a markedly slower evolution, resulting in a gradual reddening of the afterglow with time. The J-band light curve, fit with a single power law from the GROND point at 0.74 days (Kann et al. 2011; Kann & Greiner 2011) until late times, results in a best-fit decay of $\alpha_J = 0.50^{+0.04}_{-0.04}$, with a poor χ^2/dof = 39.18/6. This suggests both that the decay rate overall is much slower than in the u band, but also that a single power law is a poor fit to the available data. This poor χ^2 is predominantly caused by the flat behavior between our first *HST* observations and those with HAWK-I $\sim$5 days later. While color terms potentially create a problem here since F125W and the HAWK-I J band are not identical filters, we do not believe this is significant, since the use of secondary calibrators in each field suggests the afterglow was genuinely flat over this period, which in the rest-frame corresponds to $\sim$7–10 days post-burst. The difference in the slopes between the J band and the u band is inconsistent with a simple spectral break between the two, since we observe $\Delta\alpha = 0.86 \pm 0.07$, compared with the expectation of the cooling break of $\Delta\alpha = 0.25$. This is indicative of an additional component contributing to the optical/near-IR light at late times. In Section 7, we consider the possibility that this is an accompanying SN.

To estimate the magnitude of the host galaxy, we obtained a series of observations from Gemini-S (u, g, and r bands on 2012 June 24) and Gemini-N (J band on 2012 November 6). These provide magnitudes of $u = 25.36 \pm 0.25$, $g = 25.72 \pm 0.07$, $r = 24.94 \pm 0.06$, and $J > 24.0$ (all AB). Given the flatness of the u band between these epochs, we assume that all the magnitudes measured here are of the host galaxy. However, we note that while this seems likely for the u band (unless the afterglow has exhibited a prolonged plateau), the g- and r-band data remain on the extrapolation of the earlier afterglow (see Figure 6) and so formally these magnitudes provide only an upper limit on the host galaxy brightness.

4.3.3. GRB 121027A

GRB 121027A was observed with the Anglo Australian Telescope beginning 3.5 hr after the burst. At this epoch, imaging

with the Infrared Imaging and Spectrograph revealed the IR counterpart, which was seen to brighten over the course of the first ∼24 hr after the burst (Starling et al. 2012a; Levan et al. 2012). Follow-up observations were obtained with Gemini-S/GMOS, showing the source to be relatively blue. These observations also demonstrated that, as was the case for both GRB 101225A and GRB 111209A, the optical and X-ray light curves bear little resemblance to each other. In particular, over the timeframe during which the X-ray light curve decays by a factor of ∼10, the optical light curve in fact brightens by a factor of three. This comparison and the detailed properties of the light curves will be discussed in more detail by R. L. C. Starling et al. (in preparation).

4.4. Longer Wavelength Observations

All of the bursts discussed here have been observed at millimeter and radio wavelengths by various authors. For GRB 101225A, no radio source was detected in observations with the Jansky Very Large Array beginning on 2010 December 30 00:43 UT to a limit of 60 μJy at 5 GHz (Zauderer et al. 2011a). A second epoch obtained 2011 January 6 23:46 UT also found no source, with limits of 42 μJy and 30 μJy at 4.5 and 7.9 GHz, respectively (Frail 2011). The lack of X-ray detections at this epoch means that only optical data are available and so the resulting broadband SED is poorly constrained.

Observations of GRB 111209A also initially failed to yield any detection, with an upper limit of 132 μJy at 34 GHz being placed approximately two days after the burst (Hancock et al. 2011). However, observations taken five days post-burst did reveal a source with flux densities of 0.85 ± 0.04 mJy (5.5 GHz), 0.97 ± 0.06 mJy (9 GHz), and 3.23 ± 0.05 mJy (18 GHz) (Hancock et al. 2012). Our optical SED is poorly sampled at around this time, but aside from the steep slope between 9 and 18 GHz, the overall shape of the broadband SED is not dissimilar from the canonical expectations of a GRB afterglow at this epoch (e.g., Sari et al. 1998).

Finally, GRB 121027A was observed with the APEX/LABOCA bolometer, 4.02 days after the initial trigger. These observations failed to yield any sources to an upper limit of 21 mJy beam^{-1} (3σ, Greiner et al. 2012).

5. HOST PROPERTIES

The nature of the host galaxies can provide important clues to the possible progenitor systems of the ultra-long GRB events. For GRB 101225A and GRB 111209A, faint underlying host galaxies have been uncovered in deep, late-time imaging.[35]

The constraints on the luminosity of the host of GRB 101225A come from late-time imaging with Gemini and GTC and prior imaging of the region from the PAndAS (Thöne et al. 2011; McConnachie et al. 2009). We infer that the galaxy is faint and blue, with an absolute magnitude $M_B \approx -16.3$. It is also notably compact, being unresolved in ground- and space-based imaging, suggesting a size of <600 pc in radius. The relative sizes and absolute magnitudes of these galaxies in comparison with other GRB hosts are shown in Figure 8.

The host spectrum shows relatively strong, narrow emission lines: although the continuum is only very weakly detected, we estimate the rest-frame equivalent widths $EW_{[O\,II]} \approx 100$ Å and $EW_{[O\,III]} \approx 110$ Å and find them to be consistent with a high specific star formation rate. The lack of absorption lines, particularly Mg II, may be suggestive of a relatively small path length of cold interstellar medium (ISM) along the line of sight, but the S/N is not sufficiently high for such diagnostics to be constraining.

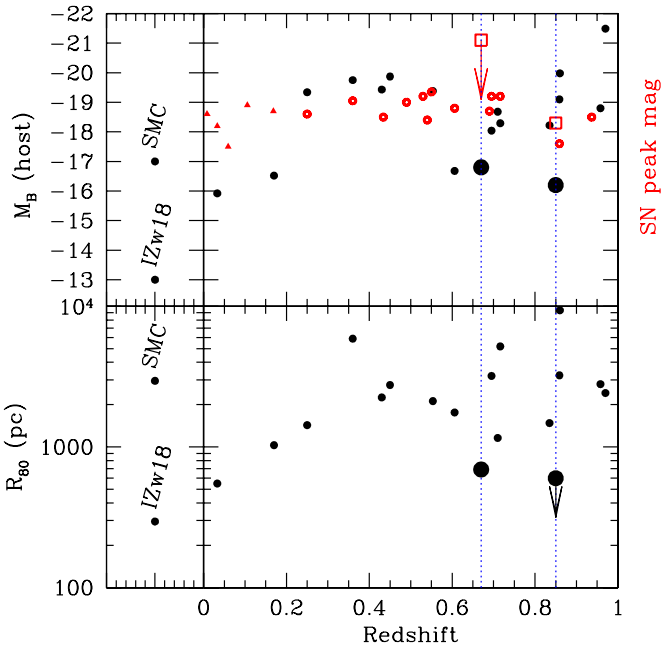

Figure 8. Constraints on the SNe and host galaxies associated with GRB 101225A and GRB 111209A, based on the observations with the Canada–France–Hawaii Telescope, Gemini, and *HST*. The top panel shows the absolute magnitudes of the host galaxies (black; Svensson et al. 2010) and SNe (red; Hjorth & Bloom 2012) associated with GRBs. The filled triangles represent firm spectroscopic associations with SNe and the open circles weaker spectroscopic or photometric SNe. The redshifts of GRB 101225A and GRB 111209A are indicated by dashed blue lines, while the open red boxes indicate the approximate magnitudes of the associated SNe, if the plateau in each light curve is ascribed entirely to SN emission. The lower panel shows the radii of several GRB hosts, compared with the limits on GRB 101225A and GRB 111209A based on the non-detection (or in the case of GRB 111209A, the marginal detection) of extension in the *HST* observations. As can be seen, the hosts of GRB 101225A and GRB 111209A are extreme in comparison with normal GRB hosts. However, similarly compact galaxies, such as IZw18 (Fiorentino et al. 2010; Aloisi et al. 1999), can be found in the local universe and so these properties are not unprecedented.

(A color version of this figure is available in the online journal.)

Given the relatively low S/N ratio, extracting measures of metallicity, such as $R_{23} = ([O\,II] + [O\,III])/\,H\beta$, is challenging, especially since Hβ is in a sky line. However, it is clear that Hβ is not unusually strong relative to the strengths of the oxygen lines and so an extremely low metallicity is unlikely.

The host galaxy of GRB 111209A is also faint ($M_B \approx -17.6$) and compact. Our *HST* imaging at five weeks has a magnitude consistent with that obtained at much later times, suggesting that we are observing the host galaxy, but this galaxy is barely resolved in the F336W image (there is a weak extension visible making the object marginally larger than the *HST* PSF; see Figure 10), again suggesting a compact size. Measuring the 80% light radius from the weak extension seen implies a size of ∼700 pc. The VLT/X-shooter spectrum shows emission lines from the host. Again, our estimate of the EWs of [O II] and [O III] are around 30–60 Å, although this is complicated by the necessity of accounting for the contribution of transient light to the latest spectrum.

Given the better S/N in this spectrum, it is possible to estimate R_{23}, although with some uncertainties as to the continuum level.

[35] It is still too early (2.5 months at the time of this writing) to uncover such a host for GRB 121027A, as it is apparently still dominated by the afterglow.

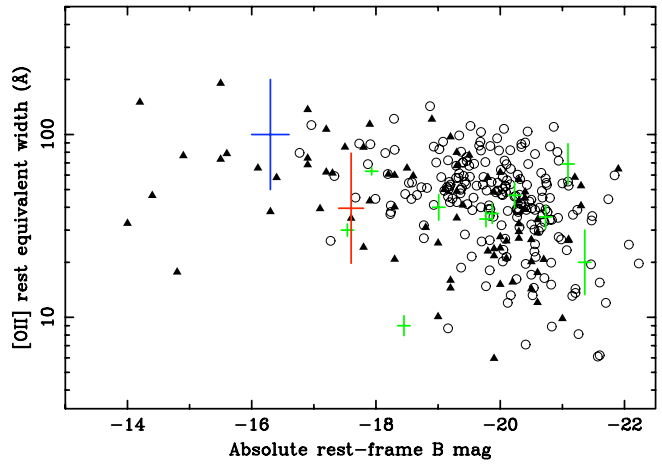

Figure 9. Properties of the two host galaxies, absolute blue magnitude vs. the EW of [O II] (GRB 101225A in blue and 111209A in red), in comparison with a sample of local blue compact dwarf galaxies from Kong et al. (2002, black triangles), moderate redshift galaxies in the GOODS field (open circles, from Kobulnicky & Kewley 2004), and a sample of pre-*Swift* GRB host galaxies (green crosses). Although the EW measurements, in particular, have rather high uncertainty, they are consistent with being members of the blue compact dwarfs, but are somewhat offset from the field galaxy sample of Kobulnicky & Kewley (2004) or the GRB host galaxies (although all samples may contain significant selection effects). The GRB host galaxy M_B values have been fit using the techniques of Perley et al. (2013) and the [O II] EWs are taken from Bloom et al. (2001, 1998), Djorgovski et al. (2001, 1998), Le Floc'h et al. (2002), Castro-Tirado et al. (2001), Piro et al. (2002), Price et al. (2002, 2003), Margutti et al. (2007), and Prochaska et al. (2004).

(A color version of this figure is available in the online journal.)

Doing so gives $\log(R_{23}) \sim 1.0$, corresponding to a metallicity of $12+\log(\mathrm{O/H}) = 8.3 \pm 0.3$, significantly sub-solar, but not especially low.

The properties of these galaxies, in magnitude, size, and metallicity are similar to those of compact star-forming field galaxies in the same redshift range (e.g., Guzman et al. 1997) and low-luminosity blue compact dwarf galaxies in the local universe (Figure 9). In other words, they are not unprecedented, but are unusual and suggest a progenitor preferentially found in a dense, low-metallicity, intensively star-forming environment. While this sample is clearly very small, it is interesting to note that these galaxies are somewhat unusual, even when compared with GRB host galaxies (as seen in Figure 8)—they are both smaller and less luminous than the large majority of GRB hosts. Only the host of the low-luminosity GRB 060218 appears broadly similar, given that GRB 060218 was also an exceptionally long and atypical GRB (Campana et al. 2006), this similarity may not be entirely coincidental. It could suggest a similarity in emission mechanisms between the long-duration, low-luminosity bursts and the ultra-long, but much higher luminosity events considered here.

5.1. Astrometric Constraints

A crucial diagnostic as to the nature of any transient event is its location within its host galaxy (e.g., Bloom et al. 2002; Fruchter et al. 2006; Svensson et al. 2010; Fong et al. 2010; Anderson & James 2009). Events occurring at locations inconsistent with the nucleus of the host are unlikely to be associated with accretion onto a supermassive black hole, either as AGN outbursts or TDEs (unless the black hole itself has been kicked; e.g., Komossa & Merritt 2008). Nuclear events can favor accretion onto supermassive black holes, although for individual events they do not rule out stellar scale events, such as nuclear SNe which may be much more common than tidal disruptions (Strubbe & Quataert 2009).

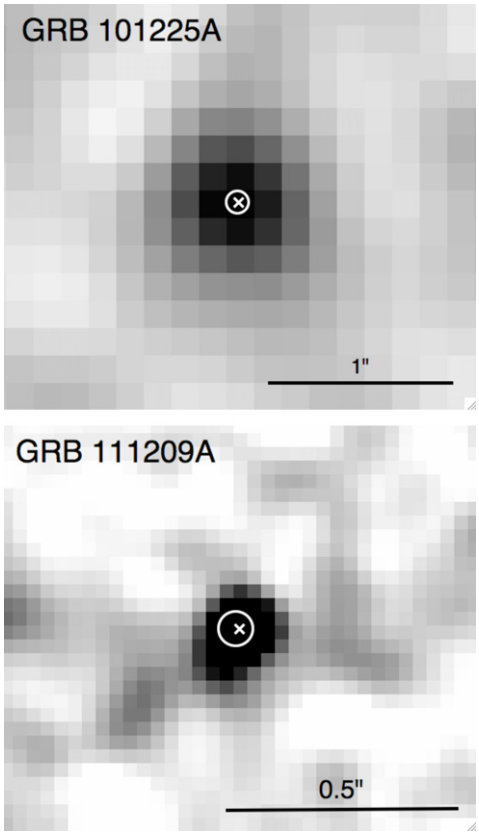

Figure 10. Astrometric constraints on the locations of GRB 101225A and GRB 111209A. In each case, the circle shows the location and associated 1σ error on the position of the afterglow, overlaid on a late-time image of the host galaxy of the GRB. The cross marks the optically determined centroid of the galaxy, determined by fitting a Gaussian profile to the host light (in each case, the hosts are at best barely resolved by the instruments (GMOS for GRB 101225A and WFC3 for GRB 111209A) and so host morphology is not important for the determination of the centroid.

To localize the GRB positions precisely on their hosts, we compare the astrometry from early observations when the afterglow is bright against the images taken at late times when the host dominates. Using 10 and 8 point sources in common for GRB 101225A (using two Gemini frames, taken in 2010 December and 2011 July) and 111209A (using the two *HST* F336W frames), respectively, we find that the offsets from the nucleus of the host galaxies in each case are ($0\farcs016 \pm 0\farcs020$) and ($0\farcs011 \pm 0\farcs038$), respectively. In other words, both sources are consistent with the nuclei of their hosts and likely lie within 150 and 250 pc of the nucleus in each case, as is shown graphically in Figure 10. However, these hosts are also extremely compact, with FWHMs that are, at best, barely resolved with *HST*. Therefore, a significant fraction of the total stellar light of these galaxies clearly also lies within the error radii associated with the astrometric transformations. The positions therefore neither rule out events associated with a supermassive black hole nor do they strongly disfavor stellar scale events, more akin to classical long GRBs, which lie at locations consistent with the nuclei of their hosts ~10% of the time (Bloom et al. 2002; Fruchter et al. 2006).

6. ENERGETICS

Based on the redshifts and light curves, we can estimate the total energy of the bursts. Doing so purely from the BAT

fluence is impractical here due to gaps in coverage of the orbit and the long-lived emission. Therefore, we integrate the energy based on the combined BAT-XRT light curves (using the method of O'Brien et al. 2006) and assuming a power-law interpolation over the orbit gaps. Integrating over the first 10^4 s (observer frame) for each burst yields isotropic energy releases of $E_{\rm iso} = 1.20 \times 10^{52}$ erg (101225A), $E_{\rm iso} = 5.21 \times 10^{52}$ erg (111209A), and $E_{\rm iso} = 7.00 \times 10^{52}$ erg (121027A). We note that given the rapid decay and poor sampling later, this number is comparable to the total energy release. The corrections to more common bands (e.g., 15–150 keV) are dependent on the spectral shape, but we note that in the case of GRB 101225A the BAT spectral slope (Palmer et al. 2010) is broadly consistent with that measured by the XRT ($\Gamma \approx 1.8$) and suggests a modest correction. For GRB 111209A, the harder spectral slope results in a correction factor, making the 15–150 keV energy a factor ~4 larger, while for GRB 121027A, the slopes are softer ($\Gamma_{\rm BAT} = 1.82 \pm 0.09$) and, as in the case of GRB 101225A, require a rather smaller correction.

These energies are relatively common for *Swift* GRBs, lying somewhat below the most extreme $E_{\rm iso}$ cases that have been observed (e.g., Racusin et al. 2008, 2009; Bloom et al. 2009; Tanvir et al. 2010). We note that while the late-time multiwavelength light curves are poorly sampled and perhaps contaminated by additional components. If we assume that the underlying mechanism for the late-time emission is similar to that for GRB afterglows, then we see no compelling evidence for jet breaks within them (the breaks to a steep decay at $\sim 10^4$ s are far too steep for a jet break). The constraints for GRB 101225A are weak, since it was not detected after the rapid decay. For GRB 111209A and GRB 121027A, the XRT observations continue until $\sim 2 \times 10^6$ s and suggest that any jet break occurs after this time. In practice, the data are only weakly sensitive to breaks close to the end of these observations (e.g., Racusin et al. 2009), due to the limited lever arm provided at late times. Coupled with this, more realistic simulations of GRB jet evolution suggest that for many viewing angles (those not directly on-axis), the jet break is effectively smeared out, making its detection extremely challenging (van Eerten et al. 2011; van Eerten & MacFadyen 2012). Nonetheless, for canonical jet parameters in simple models (e.g., Frail et al. 2001), it is possible to place limits on the jet opening angle of $\theta_j > 12$ deg (111209A) and $\theta_j > 10$ deg (121027A). The resulting beaming-corrected energies are $E_\gamma > 1.2 \times 10^{51}$ erg (111209A) and $E_\gamma > 1.0 \times 10^{51}$ erg (121027), again entirely in keeping with the energy output of many long-duration GRBs (e.g., Frail et al. 2001; Berger et al. 2003; Bloom et al. 2003; Racusin et al. 2009).

7. DISCUSSION AND INTERPRETATION

We are now poised to address the nature of these ultra-long GRBs and hereafter will concentrate on GRB 101225A and 111209A, as they are better monitored than GRB 121027A and at a redshift at which much stronger constraints can be placed on their progenitors. The nature of GRB 101225A has already generated a good deal of controversy. Until this work, it has not been clear if it belonged to the extragalactic GRB population (Thöne et al. 2011) or some new population of transients within the Milky Way, perhaps originating from tidal disruptions of asteroids by a neutron star (Campana et al. 2011), interestingly one of the models that was first proposed for GRB production (Newman & Cox 1980; Colgate & Petschek 1981). Below, we discuss various possibilities for the origin of these extremely long GRBs.

7.1. A Core Collapse Origin?

It is now clear that the vast majority of long-duration GRBs are due to stellar core collapse, which also produces an accompanying SN explosion (see Hjorth et al. 2003; Stanek et al. 2003; Hjorth & Bloom 2012, but see also Fynbo et al. 2006; Gal-Yam et al. 2006; Della Valle et al. 2006; Ofek et al. 2007 for rare possible counter examples). In each case that has been spectroscopically confirmed, the SN appears as a broad-lined SN Ic, suggestive of a stripped and compact progenitor. In the standard collapsar model, the central engine must be active for a sufficient amount of time for the nascent jet to break out of the progenitor (Woosley 1993; Bromberg et al. 2012), with the γ-ray duration being the lifetime of the jet *after* it has penetrated the stellar envelope. The signature of this—a flat distribution of durations when the γ-ray duration is less than the breakout time—has been seen in *Swift* bursts (Bromberg et al. 2012), directly implying that most arise from compact progenitors. This lifetime is also natural for material accreting onto the nascent black hole from immediately outside the innermost stable orbit. However, these durations are incompatible with red supergiant progenitors, which pre-explosion imaging ties to the SN II-P (Smartt et al. 2009) since their typical radii are 100 to almost 1000 $R_\odot$. Any moderately relativistic jet would require $R_*/c > 500$ s to tunnel through a red supergiant and so would need a very fine tuned engine to subsequently create GRBs with durations of only a few seconds. Even if accretion-driven engines were present in a significant fraction of SNe, they would be choked by the progenitor envelope and either no or a rather weak GRB might be seen. Such a scenario has been suggested as a plausible explanation for the low-luminosity GRBs (Bromberg et al. 2011), which, while weak in γ-rays, often host SNe very similar to those seen in the prototypical SN/GRB 030329 (e.g., Hjorth et al. 2003; Pian et al. 2006), while population III stars might also suffer from similar constraints (e.g., Nakauchi et al. 2012). Therefore, a requirement for jetted events from stars of large radius is significant late-time engine activity that can power the jet. This is likely to arise from ongoing (fallback) accretion onto the nascent compact object.

At first sight, it would appear that these two bursts are promising candidates for engines in stars with larger radii. This might naturally explain the long durations since these larger stars also have a reservoir of material at larger radii from the black hole, which could power longer-lived emission than from a compact star (Quataert & Kasen 2012; Woosley & Heger 2012; Nakauchi et al. 2013). Indeed, such an origin has been suggested recently for GRB 111209A (Levan 2012; Gendre et al. 2013). The long duration of the event comfortably provides sufficient time for the jet to penetrate a more extended star. In this model, the rapid variability is not uncommon in GRB prompt emission and the steep decay can be naturally interpreted as emission from high latitudes (Kumar & Panaitescu 2000; Zhang et al. 2006, 2007, 2009).

Equally, it should be noted that while larger stars may provide a natural explanation of the long durations of these events (and are probably more astrophysically common), the duration of the burst is intrinsically thought to be linked to the duration of the engine (e.g., Bromberg et al. 2012), not explicitly the radius of the star. Hence, while a shorter duration burst effectively rules out extended progenitors, the opposite is not true; these bursts

could arise from compact stars in which the engine has been active for an unusually long period.

7.1.1. Optical/IR Constraints on SN Emission

At redshifts of $z = 0.847$ and $z = 0.677$ for GRB 101225A and 111209A, respectively, typical SNe associated with GRBs will peak around the z and J bands and will show strong suppression shortward of the V band (3000 Å in the rest frame) due to UV metal line blanketing. The light curves of GRB 101225A and GRB 111209A are shown in Figure 6, along with expectations for an SN 1998bw-like SN. The evolving SEDs of GRB 101225A and GRB 111209A are shown in Figure 7. In both events, there is some evidence of flattening or re-brightening at late times relative to their host galaxy levels, as well as a gradual reddening in their SEDs. This may be indicative of underlying SNe, since they can flatten or reverse the afterglow decay and are typically much redder than the afterglows (which should also decay in a broadly achromatic manner). While both the reddening and flattening of the light curves of these events is clear, it should be noted that this behavior is not well matched in either timescale or peak luminosity with the expectations of SN Ib/c seen in most GRBs.

If these events are due to core-collapse SNe, but not SNe Ib/c similar to those seen in most other GRBs, then the timing of the SNe peak, its magnitude, and the underlying spectra become far less well constrained. SNe II-P (the progeny of large radii supergiants; Smartt et al. 2009) can reach peak extremely quickly, remain at a similar magnitude for ∼100 days, and exhibit blue spectra during early times in the plateau (e.g., Filippenko 1997; Arcavi et al. 2012), with pronounced blue-to-red evolution in the UV throughout (e.g., Bayless et al. 2013). SNe II-L appear to be more akin to SNe Ib/c in light-curve shape (e.g., Filippenko 1997; Arcavi et al. 2012), but also show broad Hα emission that may leave a detectable photometric signature in the band containing Hα. Finally, SNe IIn, characterized by narrow emission lines from circumstellar interaction, can also show extremely bright peak magnitudes (e.g., Smith et al. 2007). In other words, the behavior of the counterparts might be very different from those typically seen in GRBs, if the underlying SN is of a different type.

Distinguishing these possibilities within our relatively sparse data is clearly difficult. The late-time SEDs are poorly sampled, with modest photometric errors and poorly quantified contributions from ongoing afterglow emission and the underlying host galaxy (both as a source of additional flux and dust attenuation). Therefore, we do not attempt detailed fitting of SN templates, but consider the broad properties that would be expected for different SN types.

For GRB 101225A, the late-time SED is clearly inconsistent with being dominated purely by an SN 1998bw-like SN at a similar epoch (Figure 7), although the peak magnitude if the late-time i-band light was from an SN would be rather similar to SN 1998bw. In particular, it is far too blue at late times, given the redshift of $z = 0.847$. The host galaxy level appears to be well below the blue late-time flux and hence it is likely the result of either the associated SN or ongoing afterglow emission. In the former case, the SNe would need to be relatively blue, perhaps akin to the early-time (∼15 days) UV to optical spectrum of SNe II-P, such as SN 2005cs or 2012aw[36] (Pastorello et al. 2006; Brown et al. 2009; Bayless et al. 2013), although it would necessarily be much brighter with $M_V \sim -18.5$. This is rather brighter than the underluminous $M_R = -15.48$ for SN 2005cs (Pastorello et al. 2006) or $M_V \sim -17$ for SN 2012aw (Bayless et al. 2013), although bright SNe II-P do exist, e.g., SN 1992am (Schmidt et al. 1994). In the case of continuing afterglow emission, the afterglow would still have needed to redden considerably from its earlier behavior, but might have done so had the early (extremely blue, possibly thermal) emission not been related to the classical afterglow emission, but to some additional component such as the interaction with a dense envelope, as in Thöne et al. (2011).

For GRB 111209A, the spectra are clearly different from SN 1998bw at similar epochs, both in terms of their bulk colors, which appear much bluer, but also in the details of our *HST* grism spectra, which fail to show the expected broad features of an SN. These grism spectra do show a moderately broad rise around the expected position of the Hα line. It is possible that this arises from the underlying host galaxy, but it could also be the result of an H-rich SN. Unfortunately, the absence of late-time grism observations to subtract and the relatively low S/N of the observations preclude a detailed study of spectral features, since they are weakly detected and the host contribution is unknown. As with GRB 101225A, SN 2005cs provides a viable possible model if the late-time data are dominated by a single SN component (see Figure 7). Photometrically, we note that there is a notable plateau in the light curve of GRB 111209A at approximately 10–15 days after the burst in the J band. This would be early for the peak of an SN, but if it were associated with rising SN emission would imply an unusually luminous SN, with $M_V \sim -21$, close to that of the so-called superluminous SNe (and only about 0.5 mag fainter than this at the time of an expected SN peak for an SN 1998bw SN; e.g., Gal-Yam 2012). However, we also note that the rapid decay from this peak would not be expected in these events that tend to evolve more slowly. We also note that the same plateau is apparently visible in the u band and this may indicate that prolonged central engine activity is a more likely origin, although then the chromatic behavior of the light curve more generally (i.e., the blue-to-red evolution) could not be naturally explained.

7.1.2. X-Ray Constraints on SN Emission

In principle, the X-ray observations might provide a strong handle on the nature of SN emission. Early SNe breakouts can exhibit strong thermal emission, which provides both a hallmark of the SN activity and, crucially, a radius for the emitting blackbody. GRB SNe appear to show such signatures and so the presence of a blackbody component could be a strong indicator of the burst nature (Starling et al. 2012b; Sparre & Starling 2012). In the model suggested by Thöne et al. (2011), the blackbody radius inferred is only a few solar radii across and so would appear to immediately rule out the collapse of a large radius star. However, this is not without difficulties, as we have shown that the interpretation of blackbody components within the light curves is far from straightforward and that it is possible that no such components exist. Even if we allow a blackbody, the temperature is relatively poorly constrained, with both GRB 101225A and GRB 111209A allowing a lower temperature blackbody fit ($kT \sim 0.1$ keV), as well as a higher temperature model. In these low kT cases, the inferred radii are much larger (of order tens of solar radii) and so the constraints allowed on the radius of the progenitor via X-ray observations are unfortunately weak.

[36] SN 2005cs and SN 2012aw are among few SN II-P with good UV coverage via the *Swift* UVOT.

7.2. A Tidal Disruption Origin?

Taken at face value, the location of both GRB 101225A and GRB 111209A—consistent with the nuclei of their host galaxies—suggests a possible link with the supermassive black holes that may reside in their cores and could favor a tidal disruption scenario, as was the case for GRB 1110328A/Swift J1644+57 (Levan et al. 2011; Bloom et al. 2011; Burrows et al. 2011; Zauderer et al. 2011b) and has also been suggested for another extremely long transient, Swift 2058.4+0516 (Cenko et al. 2012).

All three bursts (101225A, 111209A, and 121027A) reach peak luminosities in excess of 10^{49} erg s^{-1}, higher by an order of magnitude than those seen in Swift J1644+57 and Swift J2058+0516. They also have a duration over which they are detected in γ-rays that is an order of magnitude smaller, so they are far from natural analogs. In particular, for a main sequence star of mass M_* and radius $R*$, the circular orbital period (P_T) at the tidal radius ($r_t \approx R_*(M_{\rm BH}/M_*)^{1/3}$) is $P_T \sim 10^4 M_*/M_\odot$ s (Krolik & Piran 2011). This might be considered the minimum timescale on which activity could be observed. In practice, simulations suggest that the rise time of a TDE is at least this, with activity expected for much longer ($>10^6$ s, e.g., Ayal et al. 2000; Lodato & Rossi 2011). Although the details of the orbit can create rather different events, as suggested for Swift J1644+57 (Cannizzo et al. 2011), it is extremely challenging to create TDE events in which the initial time for bound material to return is $<10^5$ s and so the timescales seen in ultra-long GRBs would seem to rule out a standard (i.e., main-sequence star) TDE.

However, the high luminosity is significantly in excess of the Eddington limit for a 10^{10} $M_\odot$ black hole. This, combined with the rapid temporal variations and the non-thermal nature of the spectra, suggests that any emission would be relativistically beamed (e.g., Bloom et al. 2011; Burrows et al. 2011; Zauderer et al. 2011b). If a jet component was present, then the variations could potentially be induced by Lens–Thirring precession (Stone & Loeb 2012), with the rapid cessation at $\sim 10^4$ s being caused by the precession of the jet out of the line of sight. In other words, the rapid apparent end to the X-ray emission could be interpreted as an effect of jet precession, rather than the engine switching off. Indeed, such suggestions have been considered as possible explanations for the long-term, possibly period dipping seen in Swift J1644+57 (Saxton et al. 2012), although the timescales seen in this case are much longer than for the ultra-long GRBs. If this was the case, then the timescale of X-ray activity would not rule out a main-sequence star disruption model. On the other hand, it has been argued that in realistic situations, the relatively low angular momentum of the disk compared with the black hole is likely to make any jet precession negligible (e.g., Nixon & King 2013), although the presence of a strong magnetic flux threading the hole might produce an extended period of jet wobbling prior to alignment of the jet to the hole spin axis, as has been proposed to explain the rapidly fluctuating light curve of Swift J1644+57 (Tchekhovskoy et al. 2013).

In the case of GRB 101225A, the early optical SEDs are extremely blue, too blue to be accounted for by standard fireball models (e.g., Thöne et al. 2011). In this case, the optical/UV may be explained by the presence of a hot disk, as expected in TDE flares (e.g., Lodato & Rossi 2011), which may explain why the optical evolution is largely decoupled from the X-ray. In the jetted emission scenario, we might expect to observe luminous radio emission, as has been the case in other relativistic TDE candidates (Zauderer et al. 2011b; Cenko et al. 2012). The radio upper limits reported in Section 4.4 show that five days after outburst, GRB 101225A had a 5 GHz flux of <0.06 mJy; at the same time, Swift J1644+57 exhibited a flux of ~ 2 mJy. Even accounting for the difference in luminosity distance (a factor of ~ 3), we would still expect to easily detect a similar source. In contrast, GRB 111209A was detected at a level (~ 1 mJy) which is broadly consistent with the extrapolation of the radio flux from Swift J1644+57 to $z = 0.667$.

If these events are TDE related, we might expect the late-time light curves to at least approximately follow the $t^{-5/3}$ power laws expected for TDEs (e.g., Rees 1988; Lodato & Rossi 2011) and roughly seen in the case of Swift J1644+57 (Levan et al. 2011; Bloom et al. 2011; Zauderer et al. 2012). While GRB 101225A is not detected after its rapid decay, the afterglow of GRB 111209A shows a late-time slope of $\alpha = 1.36 \pm 0.05$, while GRB 121027A shows a slope of $\alpha = 1.44 \pm 0.08$. These are both close to the $t^{-5/3}$ slope, but are also rather close to the typical late-time decay rates for GRB afterglows (Evans et al. 2009). While there is evidence for softening during the rapid decay of the light curve, the resulting late-time spectrum is still well fit with a power law, without the disk (blackbody) emission that might be expected from a tidal event.

It is interesting to note that the very low luminosity host galaxies of these bursts could harbor particularly low-mass black holes ($<10^5$ $M_\odot$). In these cases, the tidal radius of the hole becomes sufficiently small that degenerate stars (in particular, white dwarfs) can be shredded by the tidal field, rather than being swallowed directly. If these events were created by white dwarf disruptions, then many of the timescale concerns above are removed, since the much smaller tidal radius for a dense white dwarf leads to an orbital period at disruption of $P_T \sim 10 M_*/M_\odot$ s, while tightly bound material might have an orbital period of several thousand seconds (Krolik & Piran 2011). This scenario would also naturally explain why the host galaxies were extremely low luminosity, which is not naturally explained by the main-sequence hypothesis. These dense stars might then create rather powerful GRBs that can only occur in low-mass host galaxies (in contrast with normal tidal flares, which should be visible in all but the most massive galaxies, e.g., Kesden 2012). Interestingly, such models have been posited before, both for Swift J1644+57 (Krolik & Piran 2011), long GRBs where no SN events are seen (Lu et al. 2008; Gao et al. 2010), and previously identified very long duration, low-luminosity bursts (Shcherbakov et al. 2013). However, it remains unclear if such low-mass galaxies frequently host massive black holes at all. The identification of Swift J1644+57 with a Large Magellanic Cloud-like host galaxy (Levan et al. 2011) and the recent identification of a compact X-ray and radio source in Henize 2–10 (Reines et al. 2011) implies that some low-mass galaxies do harbor such black holes, but their ubiquity (and hence the rate at which they may tidally shred stars) remains highly uncertain.

Ultimately, distinguishing between SN or tidal flare origins is likely to require either an event sufficiently close that unambiguous SN signatures can be uncovered in its spectrum or, perhaps more likely, the building of a sufficiently large sample of events that the locations relative to the nuclei of their hosts can be robustly ascertained.

8. OTHER POSSIBLE EXAMPLES OF THE SAME CLASS OF EVENTS

The previous and existing GRB missions, including *Swift*, are not ideal for detecting very long-duration events. Most earlier

missions rely on rate triggers and so are at a disadvantage for longer-lived, but lower luminosity, outbursts. Moreover, *Swift* is in low Earth orbit and therefore most sources are only visible for about 45 minutes each orbit. In practice, *Swift* tends to dwell on multiple pointings each orbit, again reducing its efficiency for detecting very long events, which, of course, typically are detected as "image" triggers. However, it is plausible that some very long events can trigger the satellite on shorter timescales, for example when the light-curve morphology is such that brighter sections of the prompt emission attain sufficient brightness to enable shorter image triggers or rate triggers (e.g., GRB 121027A). In any case, the above concerns make it clear that relying on a γ-ray duration alone (especially from *Swift*) is not a good route to identifying samples of extremely long bursts.

Given this, we have searched the existing *Swift* XRT repository for examples of X-ray light curves that may show similar morphology. Such a search is not trivial since X-ray light curves already exhibit a broad diversity and many also show evidence for late-time activity, typically as flares found within the first $\sim$1000 s or long-lived plateaus lasting for longer (e.g., Burrows et al. 2005; Zhang et al. 2006). This naturally means that firmly identifying examples will be difficult, although there are certain features in the light curves of the bursts discussed here that do merit attention. In particular, three things are striking about the X-ray light curves of both GRB 101225A and GRB 111209A and so we have used these to ascertain plausible candidates. The crucial criteria are (1) long-lived X-ray emission, lasting to $\sim 10^4$ s post-burst, within two orders of magnitude of the peak, (2) a rapid decay at the end of the plateau, faster than the post-jet break expectations; we set $\alpha > 3$ as a constraint, and (3) rapid variations (dips) within the X-ray plateau of at least a factor of five. We therefore identify a sample of bursts that meet some of these criteria and, based on their light-curve morphology alone, classify them as either bronze, silver, or gold candidates if they have one (bronze), two (silver), or three (gold) of the criteria above. We note that orbit gaps and intrinsically faint afterglows mean that events that do not show all of the necessary features may still lie within a similar morphological class.

Our search revealed one notable event in the gold category, that of GRB 051117A (Goad et al. 2007). This burst shows bright X-ray emission, in excess of 10^{-9} erg s^{-1} cm^{-2} for several thousand seconds post-burst, and also exhibits at least one strong and narrow dip lasting for only a few hundred seconds. This is followed by a steep break to a decay index of $\alpha_2 = 5.38^{+2.62}_{-0.40}$, before settling into a more typical decay of $\alpha_3 = 0.92 \pm 0.04$. There is no known redshift for GRB 051117A, but the resemblance to GRB 111209A is striking. We also note that GRB 051117A is an extremely long burst as measured by the BAT, with a duration >150 s, with some evidence of much later time emission (Palmer et al. 2005). We therefore regard GRB 051117A as a likely member of this class of extremely long GRBs.

We also identify several bursts that meet two of the criteria outlined above; GRBs 111229A, 111016A, 091024, and 060607A are of particular interest. GRB 060607A lies at $z = 3.082$ and has $t_{90} = 100 \pm 5$ s (Ziaeepour et al. 2008). GRB 091024 has an extreme duration of $t_{90} \approx 1000$ s measured by *Swift*/BAT and *Fermi*/Gamma-ray Burst Monitor (Gruber et al. 2011) and was found to be at a redshift of $z = 1.09$ (Cucchiara et al. 2009). GRB 111016A has a duration of $t_{90} = 550 \pm 105$ s, but with possible long-lived emission beyond the point at which the burst left the BAT field of view. GRB 111229A had a shorter prompt duration, at $t_{90} \approx 25$ s, and was at $z = 1.38$ (Cucchiara et al. 2011). All of these bursts are apparently more distant than either GRB 101225A or GRB 111209A.

GRB 060607A has marked similarities with GRB 101225A and GRB 111209A, although its γ-ray duration is rather more typical. In the X-ray, it exhibits a long-lived plateau persisting roughly an order of magnitude fainter than its peak X-ray flux for a duration of $\sim 10^4$ s, after which it enters a rapid decay with $\alpha = 3.45^{+0.13}_{-0.12}$. Indeed, it would lie in the gold category, aside from the lack of obvious dipping or flaring behavior beyond the first few hundred seconds. The X-ray and optical afterglows appear to be largely decoupled (Ziaeepour et al. 2008), while the host galaxy is very faint. Hjorth et al. (2012) find the host has $R > 27.92$. The source has also been observed with *HST* for an exposure of 11194 s in the F775W band with ACS/WFC. From this image, we find F775W > 30.0. This suggests that the host galaxy has $M_B > -16$; this is extremely faint, perhaps comparable with the lower redshift systems considered here.

In the case of GRB 091024, the X-ray light curve is poorly sampled, meaning the overall light-curve morphology (and, in particular, the presence of a steep decay, as in criterion 2) is poorly constrained, however there is strong evidence for rapid variability within it, which, paired with the very long duration of the prompt emission, marks it as a plausible member of this class. GRB 111016A shows marked flaring, punctuated by rapid dips over the first 1000 s, but the *Swift* orbit gap means that the timing (and slope) of a rapid decay cannot be ascertained with confidence. In the case of GRB 111229A, the plateau is clearly visible, although both the level of variability within the plateau and the rapid decay at its end ($\alpha = 5 \pm 3$) are more poorly constrained.

There are several other bursts that meet one of the above criteria; for example, GRB 090417B had a long duration, $t_{90} > 260$ s, and exhibited a bright late-time flare at about 2000 s post-trigger (Holland et al. 2010). Thus, this population could potentially be moderately large, but it seems more likely that the majority of these are simply classical long duration GRBs, whose properties are outliers to the normal range. This becomes more notable when the luminosity of the bursts is considered. While GRB 051117A lacks a firm redshift, few bursts (including those considered above) reach luminosities $>10^{48}$ erg s^{-1} several thousand seconds after the burst. Since GRB 101225A, 111209A, and 121027A do attain this luminosity, it suggests that if the population of ultra-long bursts is significant within the *Swift* sample then the bursts considered here mark the high-luminosity (and hence potentially most easily detected and studied) end of the distribution.

Although the precise durations of these bursts are difficult to ascertain for a number of reasons (most notably because of the limited orbital visibility of *Swift*), we have plotted their approximate positions durations in Figure 1 (yellow), based on the location of the rapid decay attributed to high-latitude emission, which again demonstrates the likely presence of a reasonable population of such ultra-long bursts.

It is also possible to consider if previous missions have identified any members of this class. In particular, *BeppoSAX* and *HETE-2* were able to identify bursts with sufficient accuracy for afterglow follow-up, although X-ray follow-up typically took place on timescales of several hours at best, such that the X-ray diagnostics described above are of limited value. Nonetheless, the very long GRB 020410, detected by *BeppoSAX*

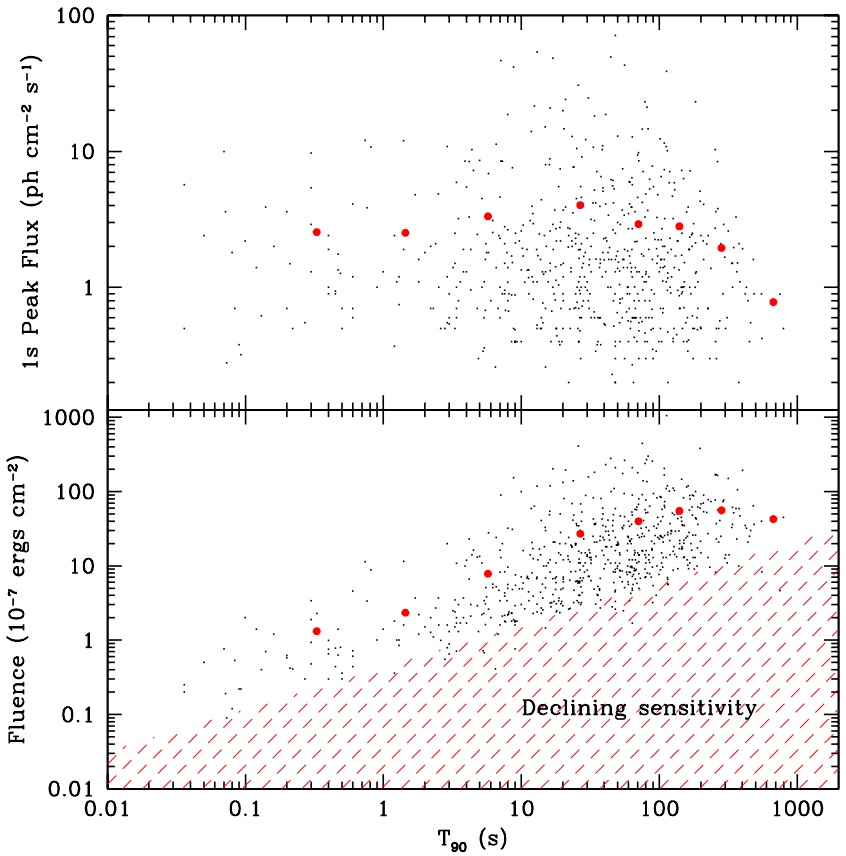

Figure 11. Constraints on the detectability of ultra-long GRBs with *Swift*. The lower panel shows the duration fluence relation (see also Levan 2012; Gendre et al. 2013), along with the median values in different duration bins (red dots), clearly showing that the longer duration bursts have on average a greater fluence; the lack of low fluence longer events suggests that this is an effect intrinsic to the detector (i.e., there is a selection against faint, long-lived transients). The upper panel shows the relation between peak flux and duration (again, red dots indicate median values), suggesting that, on average, longer bursts have fainter peak fluxes and so are less likely to result in a rate trigger for an instrument such as the *Swift* BAT.

(A color version of this figure is available in the online journal.)

(Nicastro et al. 2004), also exhibited a strong blue-to-red evolution in its afterglow and arises in a faint underlying host (Levan et al. 2005). The *HETE-2* burst 021004 exhibits a highly unusual early optical afterglow and arises from a position consistent with the nucleus of its host galaxy (Fynbo et al. 2005; Fruchter et al. 2006), while another burst GRB/XRF 030723A exhibits a late-time bump and an extremely faint host galaxy (Fynbo et al. 2004). In the latter two cases, the duration of the prompt emission is apparently much shorter, although the lack of X-ray observations limits the strength of any conclusions that may be drawn.

Finally, it is relevant to consider which of the above criteria would be needed to identify a burst as belonging to the ultra-long duration category. It is clear that identifiers of GRB type based purely on duration are crude at best. This has been studied extensively at the short-duration end, where the overlap between long and short GRBs creates significant problems in pinning down the nature of a given burst based on the prompt properties alone (Levan et al. 2007; Bromberg et al. 2012). While some attempts have been made to make such distinctions based on physical, rather than observed, properties (Zhang et al. 2009), this is difficult if one is also interested in unveiling the nature of the systems, since one cannot then use this as a diagnostic. The same is likely true at the longer duration end of the spectrum, where overlap between the longest "normal" long-GRBs and the ultra-long population will become apparent and where the sample size is sufficiently small such that it remains unclear if some properties (such as the low luminosity of the host galaxies) are simply a consequence of sample size. We therefore suggest that at present the definition of a ultra-long burst be based on the high-energy (γ-ray and X-ray) emission, following the criteria we set out above. In particular,

1. long-lived, high-energy emission, lasting to $\sim 10^4$ s after the burst;
2. rapid decay at the end of the plateau, faster than the post-jet break expectations and consistent with high-latitude emission;
3. rapid variations within the X-ray plateau emission in the form of either flares or dips, as frequently seen in prompt emission.

We do note that these criteria are not exhaustive. Indeed, recently some authors have argued that on the basis of the prompt emission only, evidence for a separate population of ultra-long GRBs is weak, demonstrating that basing classification purely on duration will not yield a clean sample (Virgili et al. 2013; Zhang et al. 2013). However, the differences in afterglow properties and weak evidence for associated SNe do suggest rather different mechanisms are at play in ultra-long GRBs from those in the "normal" population and, given their rarity, motivate a rather inclusive set of criteria for their identification. Ultimately, discerning the true nature of the ultra-long GRBs, as compared with the expectations of differing progenitor

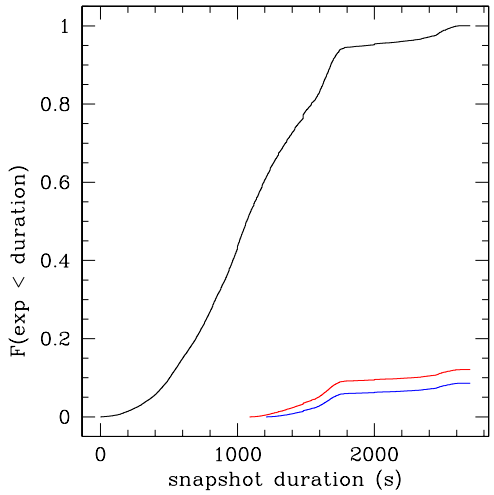

Figure 12. Distribution of *Swift* snapshot duration (i.e., the duration between slews) from 2012. The solid black line shows the cumulative fraction of the *Swift* lifetime spent in exposures longer than the snapshot duration, while the red and blue lines show the fraction of time where the longest image triggers (1088 and 1208 s) can be used, which is a very small fraction of the overall mission. This suggests that while ultra-long bursts are observationally rare, this may be largely due to a strong selection function.

(A color version of this figure is available in the online journal.)

models, will require detailed study of the rare examples that are identified.

8.1. Rates

At first glance, it would appear that *Swift* has detected at most a handful of these events over its eight-year lifespan and this would imply that events such as these are intrinsically rather rare, a conclusion reached in a separate study by Gendre et al. (2013). However, it is also important to consider that observational selection effects could act to hinder their detection. In particular, in the case of GRB 101225A, the detection was made only by integration of the fluence over a long period (over 20 minutes). Such triggers are typically sensitive only to events in which the integrated fluence is rather larger, as shown in Figure 11. The majority of bursts with durations >100 s have fluences $>10^{-7}$ erg cm^{-2}, roughly the median fluence of *Swift* GRBs. Furthermore, the peak fluxes of very long duration bursts are typically lower than for the shorter bursts, so that they are less likely to result in a rate trigger. In other words, there is a clear selection bias that *Swift* cannot detect faint, long-lived events since they simply fall below the detection thresholds for any trigger.

Furthermore, the image trigger durations can be an unusually long time for *Swift* to remain in a single pointing, in particular when long integrations (>1000 s) are needed for detection. To assess this, we plot in Figure 12 the distribution of *Swift* snapshot times (J. Kennea 2012, private communication). This shows the total fraction of the *Swift* mission that has been spent in exposures on a single source of >1088 or 1208 s (i.e., the time needed for long-image triggers to come into play). The total fraction of *Swift* observing time in such exposures in $\sim$25%. However, even in these cases the trigger is not active for the entire exposure time, since an event starting (or ending) part way through an observation, but requiring the full image trigger period to result in a detection, will not be detected (i.e., if a source that only reached the required significance in an 1088 s integration were to switch on halfway through a 1500 s exposure, it would not trigger the instrument). Hence, in the extreme, the fraction of the total exposure available for the trigger is given by the difference between the exposure time and the required trigger time ($t_{\rm exp} - t_{\rm trigger}$). This number can be seen to be rather low ($<10\%$), although such an approach is only approximate and utilizes a rather extreme example. In practice, the true fraction of the total *Swift* exposure time in which it is sensitive to ultra-long triggers is likely between 10% and 25%. For events active over several days, the limited exposure per orbit is mitigated since the exposure can be built up in subsequent orbits (e.g., Swift J2058+0516; Cenko et al. 2012), but for the ultra-long bursts (duration of hours), it suggests that the true rate to *Swift*'s fluence sensitivity could be a factor of several larger.

The long-lived, but typically low peak luminosity also suggests that bursts such as GRB 101225A and GRB 111209A may be visible over a rather restricted horizon in comparison with classical GRBs. Indeed, in a recent paper Gendre et al. (2013) suggested that GRB 111209A could be detected only out to $z \sim 1.4$, significantly below the mean redshift of GRBs (Jakobsson et al. 2012, 2006), although the detection of GRB 121027A at a much higher redshift suggests that such events can reach higher peak luminosities. Corrected for the limiting visibility window and fluence cut, it seems likely that the rate of ultra-long GRBs at a given fluence may be within a factor of a few of that of normal GRBs (with a broad range of uncertainty) and that the observed bias against their detection may simply be due to observational selection effects. If a similar beaming angle is assumed, then the true astrophysical rates would equally imply progenitors that were a factor of several rarer than for classical long GRBs (although beaming is poorly constrained in these systems). This in itself may provide some constraints on progenitor models as they cannot be such unusual systems that their rates are significantly below those of jet-powered collapsars.

9. CONCLUSIONS

We have provided evidence that several extremely long-duration transient events, in particular GRB 101225A and GRB 111209A, have very similar properties and originated in very similar galaxies. They have extremely similar X-ray light curves and luminous optical and UV emission and arise from locations close to the cores of compact, yet actively star-forming galaxies. In all of these properties (duration, X-ray light-curve luminosity/morphology, UV luminosity, host properties), these GRBs appear as outliers to the bulk of the GRB population now being observed by *Swift*. We argue that this likely reflects diversity not only in the emission properties of GRBs, but also in their progenitors. These bursts have engines that are apparently highly active (i.e., luminous γ-ray producing) for an order of magnitude longer than is possible in most GRBs. This may naturally be explained by the collapse of stars of much larger radii than the stripped envelope progenitors of most GRBs, which create powerful SNe Ib/c. Indeed, the late-time afterglows of these bursts are broadly inconsistent with those of SNe Ic and may originate from H-rich supergiants, although evidence in this direction remains sparse at present.

In any case, it is clear that these newly uncovered long-duration transients add significant diversity to the high-energy transient population, either in terms of emission mechanisms or progenitors (or both). This diverse population may not be intrinsically rare, rather the paucity of detections to date may be due to the low sensitivity of past generations of instruments to long-lived, low-flux events.

Observations to date do not offer a strong confirmation or rejection of either a core collapse or tidal disruption origin for these extremely long GRBs. Clearly, local events in which SN signatures can be searched for spectroscopically could be extremely important. However, of equal importance is the accumulation of a larger sample, whose astrometric coincidence with their host nuclei can be assessed to determine if they are consistent with an origin in supermassive black holes.

We thank D. A. Kann and the GROND team for sharing their photometric calibration and Jamie Kennea for providing information on the *Swift* slew strategy. A.J.L. acknowledges support from the Science and Technology Facilities Council (STFC, under grant ID ST/I001719/1) and is grateful to the Leverhulme Trust for a Philip Leverhulme Prize award. N.R.T., K.W., and P.T.O. thank STFC for support (grant ID ST/H001972/1). R.L.C.S. is supported by a Royal Society Dorothy Hodgkin Fellowship. The Dark Cosmology Centre is supported by the DNRF. Based on observations made with ESO Telescopes at the La Silla Paranal Observatory under programme ID 288.D-5027. Support for programs 11734, 12438, and 12786 was provided by NASA through a grant from the Space Telescope Science Institute, which is operated by the Association of Universities for Research in Astronomy, Inc., under NASA contract NAS 5-26555. Support for D.P. is provided by NASA through Hubble Fellowship grant HST-HF-51296.01-A awarded by the Space Telescope Science Institute (STScI), which is operated by the Association of Universities for Research in Astronomy (AURA), Inc., for NASA, under contract NAS 5-26555. Based on observations obtained at the Gemini Observatory, which is operated by the Association of Universities for Research in Astronomy, Inc., under a cooperative agreement with the NSF on behalf of the Gemini partnership: the National Science Foundation (United States), the National Research Council (Canada), CONICYT (Chile), the Australian Research Council (Australia), Ministério da Ciência, Tecnologia e Inovação (Brazil), and Ministerio de Ciencia, Tecnología e Innovación Productiva (Argentina). These observations were obtained as part of programme IDs GN-2010B-Q-7, GN-2011A-Q-4, GS-2011B-Q-7, GN-2011B-Q-34, and GS-2012A-Q-25. This work was made possible by contributions from Iniciativa Cientifica Milenio grant P10-064-F (Millennium Center for Supernova Science), with input from "Fondo de Innovación para la Competitividad, del Ministerio de Economía, Fomento y Turismo de Chile," and Basal-CATA (PFB-06/2007). R.A.M.J.W. is supported by the ERC through advanced investigator grant no. 247295. Partly based on observations made with the Gran Telescopio Canarias (GTC) at the Spanish Observatorio del Roque de los Muchachos of the Instituto de Astrofsica de Canarias, La Palma under programme GTC43-11B, PI: C.C. Thöne. A.dUP acknowledges support by the European Commission under the Marie Curie Career Integration Grant programme (FP7-PEOPLE-2012-CIG 322307). C.C.T., J.G., and R.S.R. acknowledge support from AYA2010-21887-C04-01 (Estallidos) and AYA2011-24780/ESP. Observations reported here were obtained at the MMT Observatory, a joint facility of the Smithsonian Institution and the University of Arizona. This work made use of data supplied by the UK Swift Science Data Centre at the University of Leicester. S.C. and G.T. acknowledge support from ASI grant I/004/11/0. S.B.C. acknowledges generous financial assistance from Gary & Cynthia Bengier, the Richard and Rhoda Goldman Fund, the Christopher R. Redlich Fund, NASA/*Swift* grants NNX10AI21G and NNX12AD73G, the TABASGO Foundation, and NSF grant AST-1211916. J.P.O. acknowledges support from the UK Space Agency. E.B. acknowledges support from the National Science Foundation under Grant AST-1107973 and from NASA/Swift AO7 grant NNX12AD69G.

REFERENCES

Aloisi, A., Tosi, M., & Greggio, L. 1999, AJ, 118, 302
Anders, E., & Grevesse, N. 1989, GeCoA, 53, 197
Anderson, J. P., & James, P. A. 2009, MNRAS, 399, 559
Arcavi, I., Gal-Yam, A., Cenko, S. B., et al. 2012, ApJL, 756, L30
Ayal, S., Livio, M., & Piran, T. 2000, ApJ, 545, 772
Balucinska-Church, M., & McCammon, D. 1992, ApJ, 400, 699
Barthelmy, S. D., Baumgartner, W. H., Cummings, J. R., et al. 2012, GCN, 13910, 1
Bayless, A. J., Pritchard, T., Roming, P. W. A., et al. 2013, ApJ, 764, 13
Berger, E., Kulkarni, S. R., & Frail, D. A. 2003, ApJ, 590, 379
Bloom, J. S., Djorgovski, S. G., & Kulkarni, S. R. 2001, ApJ, 554, 678
Bloom, J. S., Djorgovski, S. G., Kulkarni, S. R., & Frail, D. A. 1998, ApJL, 507, L25
Bloom, J. S., Frail, D. A., & Kulkarni, S. R. 2003, ApJ, 594, 674
Bloom, J. S., Kulkarni, S. R., & Djorgovski, S. G. 2002, AJ, 123, 1111
Bloom, J. S., Perley, D. A., Li, W., et al. 2009, ApJ, 691, 723
Bloom, J. S., Giannios, D., Metzger, B. D., et al. 2011, Sci, 333, 203
Bromberg, O., Nakar, E., & Piran, T. 2011, ApJL, 739, L55
Bromberg, O., Nakar, E., Piran, T., & Sari, R. 2012, ApJ, 749, 110
Brown, P. J., Holland, S. T., Immler, S., et al. 2009, AJ, 137, 4517
Bufano, F., Pian, E., Sollerman, J., et al. 2012, ApJ, 753, 67
Burrows, D. N., Kennea, J. A., Ghisellini, G., et al. 2011, Natur, 476, 421
Burrows, D. N., Romano, P., Falcone, A., et al. 2005, Sci, 309, 1833
Campana, S., Lodato, G., D'Avanzo, P., et al. 2011, Natur, 480, 69
Campana, S., Mangano, V., Blustin, A. J., et al. 2006, Natur, 442, 1008
Cannizzo, J. K., Troja, E., & Lodato, G. 2011, ApJ, 742, 32
Castro-Tirado, A. J., Sokolov, V. V., Gorosabel, J., et al. 2001, A&A, 370, 398
Cenko, S. B., Krimm, H. A., Horesh, A., et al. 2012, ApJ, 753, 77
Chapman, R., Tanvir, N. R., Priddey, R. S., & Levan, A. J. 2007, MNRAS, 382, L21
Chornock, R., Berger, E., Levesque, E. M., et al. 2010a, arXiv:1004.2262
Chornock, R., Marion, G. H., Narayan, G., Berger, E., & Soderberg, A. M. 2010b, GCN, 11507, 1
Christensen, L., Fynbo, J. P. U., Prochaska, J. X., et al. 2011, ApJ, 727, 73
Colgate, S. A., & Petschek, A. G. 1981, ApJ, 248, 771
Cucchiara, A., Fox, D., & Tanvir, N. 2009, GCN, 10065, 1
Cucchiara, A., Levan, A. J., & Tanvir, N. 2011, GCN, 12777, 1
Della Valle, M., Chincarini, G., Panagia, N., et al. 2006, Natur, 444, 1050
Dezalay, J.-P., Atteia, J.-L., Barat, C., et al. 1997, ApJL, 490, L17
Djorgovski, S. G., Frail, D. A., Kulkarni, S. R., et al. 2001, ApJ, 562, 654
Djorgovski, S. G., Kulkarni, S. R., Bloom, J. S., et al. 1998, ApJL, 508, L17
Evans, P. A., Beardmore, A. P., Page, K. L., et al. 2007, A&A, 469, 379
Evans, P. A., Beardmore, A. P., Page, K. L., et al. 2009, MNRAS, 397, 1177
Filippenko, A. V. 1997, ARA&A, 35, 309
Fiorentino, G., Contreras Ramos, R., Clementini, G., et al. 2010, ApJ, 711, 808
Fong, W., Berger, E., & Fox, D. B. 2010, ApJ, 708, 9
Frail, D. A. 2011, GCN, 11550, 1
Frail, D. A., Kulkarni, S. R., Sari, R., et al. 2001, ApJL, 562, L55
Fruchter, A. S., Levan, A. J., Strolger, L., et al. 2006, Natur, 441, 463
Fynbo, J. P. U., Gorosabel, J., Smette, A., et al. 2005, ApJ, 633, 317
Fynbo, J. P. U., Sollerman, J., Hjorth, J., et al. 2004, ApJ, 609, 962
Fynbo, J. P. U., Watson, D., Thöne, C. C., et al. 2006, Natur, 444, 1047
Gal-Yam, A. 2012, Sci, 337, 927
Gal-Yam, A., Fox, D. B., Price, P. A., et al. 2006, Natur, 444, 1053
Gao, H., Lu, Y., & Zhang, S. N. 2010, ApJ, 717, 268
Gehrels, N., Chincarini, G., Giommi, P., et al. 2004, ApJ, 611, 1005
Gendre, B., Stratta, G., Atteia, J. L., et al. 2013, ApJ, 766, 30
George, I. M., Turner, T. J., Netzer, H., et al. 1998, ApJS, 114, 73
Giblin, T. W., Connaughton, V., van Paradijs, J., et al. 2002, ApJ, 570, 573
Goad, M. R., Page, K. L., Godet, O., et al. 2007, A&A, 468, 103
Golenetskii, S., Aptekar, R., Mazets, E., et al. 2011, GCN, 12663, 1
Greiner, J., Belloche, A., Csengeri, T., et al. 2012, GCN, 13937, 1
Gruber, D., Krühler, T., Foley, S., et al. 2011, A&A, 528, A15
Guzman, R., Gallego, J., Koo, D. C., et al. 1997, ApJ, 489, 559
Hancock, P. J., Murphy, T., Gaensler, B., & Zauderer, A. 2011, GCN, 12664, 1
Hancock, P. J., Murphy, T., Gaensler, B., & Zauderer, A. 2012, GCN, 12804, 1
Hjorth, J., & Bloom, J. S. 2012, in The Gamma-Ray Burst—Supernova Connection (Cambridge: Cambridge Univ. Press), 169

Hjorth, J., Malesani, D., Jakobsson, P., et al. 2012, ApJ, 756, 187
Hjorth, J., Sollerman, J., Møller, P., et al. 2003, Natur, 423, 847
Holland, S. T., Sbarufatti, B., Shen, R., et al. 2010, ApJ, 717, 223
Ioka, K., Kobayashi, S., & Zhang, B. 2005, ApJ, 631, 429
Jakobsson, P., Hjorth, J., Malesani, D., et al. 2012, ApJ, 752, 62
Jakobsson, P., Levan, A., Fynbo, J. P. U., et al. 2006, A&A, 447, 897
Kalberla, P. M. W., Burton, W. B., Hartmann, D., et al. 2005, A&A, 440, 775
Kann, D. A., & Greiner, J. 2011, GCN, 12656, 1
Kann, D. A., Klose, S., Kruehler, T., & Greiner, J. 2011, GCN, 12647, 1
Kesden, M. 2012, PhRvD, 85, 024037
Kobulnicky, H. A., & Kewley, L. J. 2004, ApJ, 617, 240
Komossa, S., & Merritt, D. 2008, ApJL, 683, L21
Kong, X., Cheng, F. Z., Weiss, A., & Charlot, S. 2002, A&A, 396, 503
Kouveliotou, C., Meegan, C. A., Fishman, G. J., et al. 1993, ApJL, 413, L101
Krolik, J. H., & Piran, T. 2011, ApJ, 743, 134
Kruehler, T., Tanvir, N. R., de Ugarte Postigo, A., et al. 2012, GCN, 13930, 1
Kumar, P., & Panaitescu, A. 2000, ApJL, 541, L51
Le Floc'h, E., Duc, P.-A., Mirabel, I. F., et al. 2002, ApJL, 581, L81
Levan, A. 2012, in IAU Symp. 279, The Death of Massive Stars: Supernovae and Gamma-Ray Bursts, ed. P. W. A. Roming, N. Kawai, & E. Pian (Cambridge: Cambridge Univ. Press), 95
Levan, A., Nugent, P., Fruchter, A., et al. 2005, ApJ, 624, 880
Levan, A. J., Jakobsson, P., Hurkett, C., et al. 2007, MNRAS, 378, 1439
Levan, A. J., Starling, R., Tanvir, N. R., et al. 2012, GCN, 13920, 1
Levan, A. J., Tanvir, N. R., Cenko, S. B., et al. 2011, Sci, 333, 199
Liang, E., Zhang, B., Virgili, F., & Dai, Z. G. 2007, ApJ, 662, 1111
Lodato, G., & Rossi, E. M. 2011, MNRAS, 410, 359
Lu, Y., Huang, Y. F., & Zhang, S. N. 2008, ApJ, 684, 1330
Margutti, R., Chincarini, G., Covino, S., et al. 2007, A&A, 474, 815
Marshall, F. E., & Evans, P. A. 2012, GCN, 13932, 1
McConnachie, A. W., Irwin, M. J., Ibata, R. A., et al. 2009, Natur, 461, 66
Nakauchi, D., Kashiyama, K., Suwa, Y., & Nakamura, T. 2013, ApJ, 778, 67
Nakauchi, D., Suwa, Y., Sakamoto, T., Kashiyama, K., & Nakamura, T. 2012, ApJ, 759, 128
Newman, M. J., & Cox, A. N. 1980, ApJ, 242, 319
Nicastro, L., in't Zand, J. J. M., Amati, L., et al. 2004, A&A, 427, 445
Nixon, C., & King, A. 2013, ApJ, 765, 7
O'Brien, P. T., Willingale, R., Osborne, J., et al. 2006, ApJ, 647, 1213
Ofek, E. O., Cenko, S. B., Gal-Yam, A., et al. 2007, ApJ, 662, 1129
Palmer, D., Barbier, L., Barthelmy, S., et al. 2005, GCN, 4289, 1
Palmer, D. M., Barthelmy, S. D., Baumgartner, W. H., et al. 2010, GCN, 11500, 1
Palmer, D. M., Barthelmy, S. D., Baumgartner, W. H., et al. 2011, GCN, 12640, 1
Pal'Shin, V., Aptekar, R., Frederiks, D., et al. 2008, in GAMMA-RAY BURSTS 2007: Proc. of the Santa Fe Conf., AIP Conf. Ser. 1000, ed. M. Galassi, D. Palmer, & E. Fenimore (Melville, NY: AIP), 117
Pastorello, A., Sauer, D., Taubenberger, S., et al. 2006, MNRAS, 370, 1752
Perley, D. A., Levan, A. J., Tanvir, N. R., et al. 2013, ApJ, 778, 128
Pian, E., Mazzali, P. A., Masetti, N., et al. 2006, Natur, 442, 1011
Piro, L., Frail, D. A., Gorosabel, J., et al. 2002, ApJ, 577, 680
Price, P. A., Kulkarni, S. R., Berger, E., et al. 2002, ApJL, 571, L121
Price, P. A., Kulkarni, S. R., Berger, E., et al. 2003, ApJ, 589, 838
Prochaska, J. X., Bloom, J. S., Chen, H.-W., et al. 2004, ApJ, 611, 200
Qin, Y., Liang, E.-W., Liang, Y.-F., et al. 2013, ApJ, 763, 15
Quataert, E., & Kasen, D. 2012, MNRAS, 419, L1
Racusin, J. L., Karpov, S. V., Sokolowski, M., et al. 2008, Natur, 455, 183
Racusin, J. L., Liang, E. W., Burrows, D. N., et al. 2009, ApJ, 698, 43
Rees, M. J. 1988, Natur, 333, 523
Reines, A. E., Sivakoff, G. R., Johnson, K. E., & Brogan, C. L. 2011, Natur, 470, 66
Sari, R., Piran, T., & Narayan, R. 1998, ApJL, 497, L17
Saxton, C. J., Soria, R., Wu, K., & Kuin, N. P. M. 2012, MNRAS, 422, 1625
Schlafly, E. F., & Finkbeiner, D. P. 2011, ApJ, 737, 103
Schmidt, B. P., Kirshner, R. P., Eastman, R. G., et al. 1994, AJ, 107, 1444
Schmidt, G. D., Weymann, R. J., & Foltz, C. B. 1989, PASP, 101, 713
Serino, M., Nakahira, S., Negoro, H., et al. 2012, GCN, 13908, 1
Shcherbakov, R. V., Pe'er, A., Reynolds, C. S., et al. 2013, ApJ, 769, 85
Smartt, S. J., Eldridge, J. J., Crockett, R. M., & Maund, J. R. 2009, MNRAS, 395, 1409
Smith, N., Li, W., Foley, R. J., et al. 2007, ApJ, 666, 1116
Soderberg, A. M., Kulkarni, S. R., Berger, E., et al. 2004, Natur, 430, 648
Soderberg, A. M., Kulkarni, S. R., Nakar, E., et al. 2006, Natur, 442, 1014
Sparre, M., & Starling, R. L. C. 2012, MNRAS, 427, 2965
Stanek, K. Z., Matheson, T., Garnavich, P. M., et al. 2003, ApJL, 591, L17
Starling, R. L. C., Levan, A. J., Wiersema, K., et al. 2012a, GCN, 13911, 1
Starling, R. L. C., Page, K. L., Pe'Er, A., Beardmore, A. P., & Osborne, J. P. 2012b, MNRAS, 427, 2950
Starling, R. L. C., Wiersema, K., Levan, A. J., et al. 2011, MNRAS, 411, 2792
Stone, N., & Loeb, A. 2012, PhRvL, 108, 061302
Strubbe, L. E., & Quataert, E. 2009, MNRAS, 400, 2070
Svensson, K. M., Levan, A. J., Tanvir, N. R., Fruchter, A. S., & Strolger, L.-G. 2010, MNRAS, 405, 57
Tanvir, N. R., Evans, P. A., Littlejohns, O. M., & Levan, A. J. 2011, GCN, 11570, 1
Tanvir, N. R., Rol, E., Levan, A. J., et al. 2010, ApJ, 725, 625
Tanvir, N. R., Wiersema, K., Levan, A. J., et al. 2012, GCN, 13929, 1
Tchekhovskoy, A., Metzger, B. D., Giannios, D., & Kelley, L. Z. 2013, MNRAS
Thöne, C. C., de Ugarte Postigo, A., Fryer, C. L., et al. 2011, Natur, 480, 72
Tikhomirova, Y. Y., & Stern, B. E. 2005, AstL, 31, 291
van Eerten, H. J., & MacFadyen, A. I. 2012, ApJ, 751, 155
van Eerten, H. J., MacFadyen, A. I., & Zhang, W. 2011, in GAMMA-RAY BURSTS 2010, AIP Conf. Ser. 1358, ed. J. E. McEnery, J. L. Racusin, & N. Gehrels (Melville, NY: AIP), 173
Virgili, F. J., Mundell, C. G., Pal'shin, V., et al. 2013, ApJ, 778, 54
Vreeswijk, P., Fynbo, J., & Melandri, A. 2011, GCN, 12648, 1
Wiersema, K., Tanvir, N., & Levan, A. 2010, GCN, 11502, 1
Woosley, S. E. 1993, ApJ, 405, 273
Woosley, S. E., & Heger, A. 2012, ApJ, 752, 32
Zauderer, A., Berger, E., & Fong, W. 2011a, GCN, 11770, 1
Zauderer, B. A., Berger, E., Margutti, R., et al. 2012, arXiv:1212.1173
Zauderer, B. A., Berger, E., Soderberg, A. M., et al. 2011b, Natur, 476, 425
Zhang, B., Fan, Y. Z., Dyks, J., et al. 2006, ApJ, 642, 354
Zhang, B., Zhang, B.-B., Virgili, F. J., et al. 2009, ApJ, 703, 1696
Zhang, B.-B., Liang, E.-W., & Zhang, B. 2007, ApJ, 666, 1002
Zhang, B.-B., Zhang, B., Liang, E.-W., & Wang, X.-Y. 2009, ApJL, 690, L10
Zhang, B.-B., Zhang, B., Murase, K., Connaughton, V., & Briggs, M. S. 2013, arXiv:1310.2540
Ziaeepour, H., Holland, S. T., Boyd, P. T., et al. 2008, MNRAS, 385, 453